Supplementary Methods

SUPPLEMENTAL MATERIALS

Fig. S6. Additional characterization of interferon signaling, anti-IFN autoantibodies, and inter-omics analysis of top-contribution cytokines and significant pathways for the severity factor, related to Figures 5 and 6.

Fig. S7. Virus-centered integrative multi-omics network of the mortality(-associated) factor (Factor 4) in PGX, related to Figure 6

Table s1. Baseline Characteristic by Clinical Trajectory Groups. p-value from chi-square test for categorical variables and Kruskal-Wallis test for continuous variables (age, SOFA score). Trajectory 1= brief length of stay; trajectory 2= intermediate length of stay; trajectory 3= intermediate length of stay with discharge limitations; trajectory 4= prolonged hospitalization; trajectory 5= fatal. 1not including asthma, 2current or former.

Table s2. Baseline Characteristic by Cohort. p-value from chi-square test for categorical variables and Kruskal-Wallis test for continuous variables (age, SOFA score). Trajectory 1= brief length of stay; trajectory 2= intermediate length of stay; trajectory 3= intermediate length of stay with discharge limitations; trajectory 4= prolonged hospitalization; trajectory 5= fatal. 1not including asthma, 2current or former.

Table s3. Analyte contributions for MCIA factors

Table s4. MCIA factors baseline and longitudinal testing

Table s5. Functional enrichment analysis of Factor 1

Table s6. Functional enrichment analysis of Factor 1, filtered for baseline TG4 and TG5 separation

Table s7. Functional enrichment analysis of Factor 4

Table s8. Functional enrichment analysis of Factor 4, filtered for baseline TG4 and TG5 separation

Table s9. Batch-effect evaluation using PVCA

RESOURCE AVAILABILITY

All requests for information regarding reagents and resources should be directed to the lead contact and will be fulfilled by the lead contact or corresponding authors.

Lead contact

Further information and requests for resources and reagents should be directed to and will be fulfilled by Dr. Leying Guan (leying.guan@yale.edu).

Materials availability

This study did not generate new unique reagents.

Data and code availability

Data files are available at ImmPort under accession number SDY1760 and dbGAP accession number phs002686.v1.p1. All analysis codes have been deposited at https://bitbucket.org/kleinstein/impacc-public-code and are publicly available. DOIs are listed in the key resources table.

EXPERIMENTAL MODEL AND STUDY PARTICIPANT DETAILS

IMPACC Cohort characteristics

The IMPACC cohort enrolled participants from 20 hospitals affiliated with 15 geographically distributed academic institutions across the U.S. Eligible participants were patients hospitalized with symptoms or signs consistent with COVID-19, which had SARS-CoV-2 infection confirmed by RT-PCR to remain in the study. The detailed study design and schedule for clinical data and biological sample collection were previously described (1, 2). Briefly, detailed clinical assessments and nasal swabs, blood, and endotracheal aspirates (intubated patients only) were collected within 72h of hospitalization (Visit 1) and on days 4, 7, 14, 21, 28 after hospital admission. If a participant required escalation of care or was readmitted to the hospital prior to Day 28, additional samples were collected within 24 and 96 hours of care escalation or readmission. If participants were discharged prior to day 14 or 28, attempts were made to collect limited clinical information and biologic samples on days 14 and/or 28 in outpatients. Disease severity was assessed using a 7-point ordinal scale based on degree of respiratory illness (*23*), modified from Beigel et al. (3). The sex of participants was determined via physician-reported sex at birth.

Sex as a biological variable

In total, the cohort used in this manuscript had 704 (61%) males and 448 (39%) females. We identified that male sex was significantly associated with the severity factor in line with males comprising a larger proportion of more severe TGs. To control for this imbalance, sex in addition to age were used as covariates in statistical testing to identify robust trends for both sexes.

Cohort definition

In this study, we used 1,152 IMPACC participants with measurements for at least one of the following assays: plasma targeted proteomics, plasma global proteomics, serum proteomics, plasma global metabolomics, PBMC transcriptomics and nasal transcriptomics. The sample processing and data generation was performed in phases (subsets of samples). The participants were divided into training and test cohorts in the following manner. In a previous IMPACC manuscript, we analyzed a subset of the IMPACC cohort (enrolled through September 2020; phase 1 and 2 of the study) to perform deep immunophenotyping of COVID-19 disease using unimodal analyses (4). This subset was used as a training cohort in the present multi-modal integrative analysis to investigate the immune and molecular signatures of SARS-CoV-2

infection across tissue compartments at systems level. One participant in this subset lacked all six assays mentioned above, it was, therefore, excluded, resulting in 1,493 sample collection events from 539 participants in the training set. Unpublished data from another subset of IMPACC cohort (enrolled after September 2020; phase 3 of the study) was used as a test cohort to validate our conclusions of systems-level COVID-19 signatures from the training cohort. Few samples of the test cohort participants were included in phases 1 and 2, which were excluded from the test set, resulting in 1,584 sample collection events from 613 participants in the test set. The data for both the training and test sets were generated in the same manner to avoid any major technical biases.

METHOD DETAILS

Sample processing and batch randomization

Biological sample collection and processing followed a standard protocol utilized by every participating academic institution. The complete IMPACC sample processing protocol was published previously (2). Briefly, blood samples (10 ml per time point) and nasal swabs (mid-turbinate) were collected at each specified time point, and blood was processed within 6 hours of collection. Whole blood was used to identify distinct immune cell populations and quantify changes in cell populations [cytometry by time-of-flight (CyTOF)], and peripheral blood mononuclear cells (PBMCs) were collected to measure gene expression (bulk transcriptomics; PBMC gene expression: PGX) over the course of COVID-19. Serum was used to characterize SARS-CoV-2–specific antibodies, including virus neutralization. Plasma was used for proteomics (Plasma proteomics targeted: PPT & global: PPG) and metabolomics (Plasma metabolomics global: PMG), and serum was used to measure soluble inflammatory mediators (e.g., cytokines and chemokines) using oligonucleotide-linked antibody detection (Olink) (Serum proteomics targeted: SPT). RNA from the nasal swab was used to assess SARS-CoV-2 viral load and to evaluate changes in immune-related upper airway epithelial gene expression (i.e., bulk transcriptomics; Nasal gene expression: NGX). To mitigate potential batching effects, a randomization procedure was developed to help ensure that longitudinal samples from the same individuals were run on the same plates and were randomly distributed across the plates. We stratified this randomization by disease severity (moderate versus severe) and age (younger versus older) with the representation of these strata across plates. In addition, we verified that race, ethnicity, gender, and site were well-represented across the plates.

Assay preparation and processing

Raw sample collection and processing was performed as defined previously (*95*) in the following sections (names in the parentheses are section names from previous work (*95*)): NGX and viral loads (Nasal viral PCR and host transcriptomics), antibody titers (Antibody correlates: titers), SPT (Serum Olink), PPG (Plasma global proteomics), PPT (Plasma targeted proteomics), PMG (Plasma global metabolomics), whole blood CyTOF (Blood CyTOF), and PGX (Peripheral Blood Mononuclear Cell transcriptomics). Additional details on PPG sample processing were recently

published (*96*). The experimental methods for these assays follow the same protocols as described in our previous work [Core Assay] and are included below for the sake of completeness.

Nasal host gene expression (NGX)

Inferior nasal turbinate swabs were placed in 1mL of Zymo-DNA/RNA shield reagent (Zymo Research). RNA was extracted from 250 µL of sample and eluted into a volume of 50ul using the KingFisher Flex sample purification system (ThermoFisher) and the quick DNA-RNA MagBead kit (Zymo Research) following the manufacturer's instructions. Each sample was extracted twice in parallel. The 2 eluted RNA samples were pooled and aliquoted into 20 µL aliquots using a Rainin Liquidator 96 pipettor for downstream RT-qPCR and RNA-sequencing.

From each nasal RNA sample, 10ul was aliquoted to a library construction plate using the Perkin Elmer Janus Workstation (Perkin Elmer, Janus II). Ribosomal depletion, cDNA synthesis, and library construction steps were performed using the Total Stranded RNA Prep with Ribo-Zero Plus kit, following the manufacturer's instructions (Illumina). All steps were automated on the Perkin Elmer Sciclone NGSx Workstation to reduce batch-to-batch variability and increase sample throughput. Final cDNA libraries were quantified using the Quant-it dsDNA High Sensitivity assay, and library insert size distribution was checked using a fragment analyzer (Advanced Analytical; kit ID DNF474). Samples, where adapter dimers constituted more than 4% of the electropherogram area, were failed before sequencing. Technical controls (K562, Thermo Fisher Scientific, cat# AM7832) were compared to expected results to ensure that batch to batch variability was minimized. Successful libraries were normalized to 10nM for sequencing.

Barcoded libraries were pooled using liquid handling robotics prior to loading. Massively parallel sequencing-by-synthesis with fluorescently labeled reversibly terminating nucleotides was carried out on the NovaSeq 6000 sequencer using S4 flowcells with a target depth of 50 million 100 base-pair paired-end reads per sample (25 million read pairs).

Nasal Viral RT-qPCR (viral load)

The RNA samples extracted from inferior nasal turbinate swabs (as described above) were used for this assay. Master mixes containing nuclease-Free water, combined primer/probe mixes, and One-Step RT-qPCR ToughMix (Quantabio) were prepared on ice, and 15 µL was dispensed in each well of a 384-reaction plate (Thermofisher) CoV-2 was quantitated using the CDC qRT-PCR assay (primers and probes from IDT). Briefly, this comprises two reactions targeting the CoV-2 nucleocapsid gene (N1 and N2) and one reaction targeting RPP30 (RP). Each batch included positive controls of plasmids containing N1/N2 and RP target sequence (2019-nCoV_N_Positive Control and Hs_RPP30 Positive Control, IDT) to allow quantitation of each transcript. Primer/probe sequences were: 2019-nCOV_N1-F GAC CCC AAA ATC AGC GAA AT, 2019-nCOV_N1-R TCT GGT TAC TGC CAG TTG AAT CTG, 2019-nCOV_N1-P ACC CCG CAT TAC GTT TGG TGG ACC, 2019-nCOV_N2-F TTA CAA ACA TTG GCC GCA AA, 2019-nCOV_N2-R GCG CGA CAT TCC GAA GAA, 2019-nCOV_N2-P ACA ATT TGC CCC CAG CGC TTC AG, RP-F AGA TTT GGA CCT GCG AGC G, RP-R GAG CGG CTG TCT CCA CAA GT and RP-P TTC TGA CCT GAA GGC TCT GCG CG. After RNA extracts were gently vortexed and added 5 µL per sample. Plates were centrifuged for 30 s at 500 × g, 4C. Quantitative polymerase chain

reaction was performed using a Quantstudio5 (Thermo Fisher) with cycling conditions:1 cycle 10 min at 50°C, followed by 3 min at 95°C, 45 cycles 3 s at 95°C, followed by 30 s at 55.0°C.

Antibody titers

Antibody levels against the recombinant receptor-binding domain (RBD) and full-length spike were measured using a research-grade ELISA (5, 6). Briefly, samples were heat-inactivated at 56°C for 1 h. 96-well plates (Thermo Fisher Lot # 4199147) were coated with 50 µL/well of RBD or spike proteins at 2 µg/mL concentration in phosphate-buffered saline (PBS; Gibco lot # 2388102) and incubated overnight at 4°C. Plates were washed 3× in an automatic plate washer (BioTek) with PBS 0.01% Tween 20 (Fisher Scientific, Cat#BP337-100, TPBS) and blocked for 1 h with 200 µL/well of 3% non-fat dry milk (Cat#AB10109-01000) prepared in TPBS. Serum samples were serially diluted (3-fold starting at 1:80 dilution) in 1% non-fat dry milk in TPBS. The blocking solution was removed, and 100 µL/well of serially diluted samples were added to the plates and incubated for 2h at 20°C. Plates were washed 3× with TPBS, and 50 µL/well of the corresponding secondary antibody, prepared in 1% non-fat dry milk in TPBS, were added for 1h at RT: Anti-human IgG (Fc specific)-Peroxidase antibody produced in goat (Sigma-Aldrich Cat#A0170); Goat anti-human IgM-HRP (SouthernBiotech Cat#2020–05); Anti-human IgA (α-chain specific)-Peroxidase antibody produced in goat (Sigma-Aldrich Cat#A0295). Plates were washed 3× with TPBS, and 100 µL/well of peroxidase substrate (SigmaFAST o-phenylenediamine dihydrochloride, Sigma-Aldrich Cat#P9187) were added for 10 min 50 µL/well of 3M hydrochloric acid (HCl, Thermo Fisher Scientific, Cat#S25856) was added to stop the reaction. Optical density (OD) was measured in a Synergy 4 (BioTek) plate reader at 490 nm. The area under the curve was calculated, considering 0.15 OD as the cutoff. Data were analyzed using Graphpad Prism 9.

Serum proteomics targeted (Olink; SPT)

Study samples were assayed in plate batch layouts following a centralized randomized scheme that we described previously (4). Three samples (IMPACC_Serum, IMPACC_Plasma, and IMPACC_Plasma_Stim) were used as IMPACC inter-plate references (Reference samples) in every plate. All samples (participant sera and reference) were subjected to PEA (Olink) multiplex assay Inflammatory panel (Olink Bioscience, Uppsala, Sweden), according to the manufacturer's instructions. This inflammatory panel included 92 proteins associated with human inflammatory conditions. An incubation master mix containing pairs of oligonucleotide-labeled antibodies to each protein was added to the samples and incubated for 16 h at 4°C. Each protein was targeted with two different epitope-specific antibodies, increasing the assay's specificity. The presence of the target protein in the sample brought the partner probes in close proximity, allowing the formation of a double-strand oligonucleotide polymerase chain reaction (PCR) target. On the following day, the extension master mix in the sample initiated the specific target sequences to be detected and generated amplicons using PCR in 96 well plates. For the detection of the specific protein, Dynamic array integrated fluidic Circuit (IFC) 96 × 96 chip was primed, loaded with 92 protein-specific primers, and mixed with sample amplicons, including three inter-plate controls (IPS) and three negative controls (NC). Real-time microfluidic qPCR was performed in Biomark (Fluidigm, San Francisco, CA) for the target protein quantification.

Plasma proteomics global (PPG)

Fifty microliters of neat plasma samples were diluted with 450 µL of water, and 25 µL of perchloric acid was added (7). After vigorous agitation, the suspension was kept at −20°C for 15 min, then centrifuged for 60 min (4°C, 3200 ×g). 390 µL of the supernatant was mixed with 40 µL of 1% trifluoroacetic acid and loaded onto a µSPE HLB plate, previously conditioned once with 300 µL methanol and twice with 500 µL of 0.1% trifluoroacetic acid. Proteins were eluted from the µSPE HLB plate with 100 µL of 90% acetonitrile and 0.1% trifluoroacetic acid. After elution, the samples were dried with a Speedvac, resuspended with 35 µL of 50 mM ammonium bicarbonate, and digested with 10 µL trypsin (500 ng) overnight at 37°C. Digestion was stopped by the addition of 5 µL 10% formic acid. The samples were stored at −80°C before LC/MS analysis. Two microliters of tryptic peptides were loaded onto Evotips and analyzed using an Evosep ONE liquid chromatography system (EVOSEP, Odense, Denmark) connected to a timsTOF Pro mass spectrometer (Bruker Daltonics, Billerica, MA, USA). The Evosep ONE was set to 60 samples per day, and the mass spectrometer was operated in DDA-PASEF mode. DDA-PASEF parameters were set as follows: m/z range 100–1700, the mobility (1/K0) range was set to 0.70–1.45 Vs./cm2, and the accumulation time was set to 100 ms.

Plasma proteomics targeted (PPT)

All chemicals and reagents were purchased at the highest purities available. Solvents used in this study were LC/MS grade and were purchased from Fisher Chemicals (Thermo Fisher Scientific). Briefly, a volume of 10 µL of 10-fold diluted plasma was mixed with 60 µL of urea buffer (8M urea in 50 mM ammonium bicarbonate, Sigma Aldrich) and 15 µL of dithiothreitol buffer (DTT, 50 mM in urea buffer, Sigma Aldrich) before incubated 30 min on a thermomixer (800 rpm, room temperature). The samples were alkylated using iodoacetamide buffer (IAA, 375 mM in urea buffer, Sigma Aldrich) and incubated for 30 min (800 rpm, room temperature, and dark). A volume of 10 µL of DTT buffer was added to quench the alkylation. The samples were transferred to the SP3 beads mixture (Sera-Mag SpeedBeads, 1:1 v/v, GE Healthcare) previously washed with HPLC water (scale 1:10 protein to beads). Then a volume of 150 µL of absolute ethanol (Supelco) was added, and the mix was incubated for 15 min on a thermomixer (1,000 rpm at room temperature). The samples were placed on the magnetic rack, and the clear supernatant was removed. The beads were washed in three cycles in 200 µL of 80% ethanol. After the final washing step, the samples were trypsinized using 100 µL of trypsin buffer (Promega, 20 µg/mL in 50 mM ammonium bicarbonate) and placed on a thermomixer (1,000 rpm, 2 h, 37°). After digestion, the samples were centrifuged to pulldown the liquid and placed on a magnetic rack to collect the supernatant and were then acidified with 2% v/v formic acid in HPLC water (Sigma Aldrich). The C18 cleanup was performed using a 96-well MACROSPIN C18 plate (TARGA, The NestGroup Inc.), and the tryptic peptides were eluted off the C18 particles using 40% ACN/0.1% FA. The samples were dried and stored at −20°C until LC/MS analysis (8). The samples were analyzed using an LC system (Nexera Mikros, Shimadzu) equipped with a Capillary C18 column (0.2 × 100mm, 2.7um particle diameter, Shimadzu) coupled online to an 8060 triple quadrupole mass spectrometer instrument (Shimadzu). From each sample, 1 µg peptide quantity was separated using a non-linear gradient over a 15-min run time operated at 10 µL/min (5% solvent B for 0.2 min; 5 to 40%B for 10.3 min; 85%B for 1.5 min and 5% for 3 min). The final scheduling

method was performed using the following parameters: 1.2 s of maximum loop time with minimum dwell time of 2 msec and pause time of 1 msec, Q1 and Q3 resolution set at the 'unit' level.

Plasma metabolomics global (PMG)

Plasma metabolite profiling was conducted by Metabolon using in-house standards (9, 10). The samples were divided into randomized sample batches, extracted, and prepared for analysis using Metabolon's solvent extraction method (Evans, 2008). Recovery standards were added to the first step in the extraction process to ensure proper quality control. Protein was removed by methanol precipitation under vigorous shaking for 2 min (Glen Mills GenoGrinder 2000) and then by centrifugation. The supernatants were divided into five fractions: two for analysis by two separate reverse phases (RP)/UPLC-MS/MS methods with positive ion mode electrospray ionization (ESI); one for analysis by RP/UPLC-MS/MS with negative ion mode ESI; one for analysis by HILIC/UPLC-MS/MS with negative ion mode ESI; and one sample was reserved for backup analysis using Waters ACQUITY ultra-performance liquid chromatography (UPLC) and a Thermo Scientific Q-Exactive high resolution/accurate mass spectrometer interfaced with a heated electrospray ionization (HESI-II) source and Orbitrap mass analyzer operated at 35,000 mass resolution. Metabolites were identified by comparison to Metabolon library entries of standard metabolites (9) based on three criteria: retention index (RI) within a narrow RI window of the proposed identification; accurate mass match to the library ±10 ppm; and the MS/MS forward and reverse scores between the experimental data and authentic standards. Compounds were categorized according to reporting standards set by the Chemical Analysis Working Group of the Metabolomics Standards Initiative (11–13), and appropriate orthogonal analytical techniques were applied to the metabolite of interest and a chemical reference standard. Metabolites were reported that had their corresponding accurate mass confirmed via MS with retention index, chemical, and composition ID.

Blood CyTOF

Samples from a given batch were acquired on the Fluidigm Helios mass cytometer in multiple acquisitions. The PROT-1 fixed whole blood samples were processed in batches of 20 samples. Due to sample quality issues, some samples remained pink or red after the barcoding step; those samples were discarded, and the remaining samples were pooled for the remaining staining steps. After staining was completed, the pooled sample was counted and split into 2–3 subsamples to be frozen as FBS/DMSO samples stored at −80C until the day of acquisition. On the day of acquisition, the Helios instrument was tuned according to the manufacturer's software standards; if the signal of Tb159 or Tm169 from the Fluidigm Tuning Solution was more than 10% lower than previous days, the process was repeated until the margin was achieved. The final Tuning results were exported as a CSV from the software for the record.

One FBS/DMSO subsample was thawed, washed once with Fluidigm Cell Staining Buffer, and then counted on a Bio-Rad TC20 cell counter. If necessary, the sample was split into subsamples of 2 × 106 cells, centrifuged, and the resulting pellet was left with a minimal overlay of CSB. One CSB subsample was washed twice in MilliQ water, or Fluidigm Cell Acquisition Solution then resuspended to 7–8 x 105/mL in CAS or MilliQ containing a 10-fold dilution of Fluidigm EQ 4-Element normalization beads and acquired on the tuned Helios instrument using either the PSI

or SuperSampler for sample introduction. This dilution was chosen to give approximately 250–350 events/sec acquisition rate. The next CSB subsample or FBS/DMSO subsample was processed when the previous sample had less than 1mL of sample remaining. The instrument was cleaned with Fluidigm Wash Solution whenever clogging occurred, or approximately every 2 × 106 cell events were acquired. These cleaning steps resulted in multiple FCS files per pooled sample acquisition. Pooled samples were acquired until a total of 6 × 106 cell events had been collected, or all FBS/DMSO samples were collected, whichever occurred first. This corresponds to an average target event number of 3 × 105 events per original donor subsample.

Peripheral blood mononuclear cell (PBMC) gene expression (PGX)

RNA was extracted from cells (2.5 × 105 PBMCs) homogenized in 200 µL of Buffer RLT (Qiagen) and then extracted using the Quick-RNA MagBead Kit (Zymo) with DNase digestion. RNA quality was quantitated using Qubit HS RNA assays and assessed using a Fragment Analyzer (Agilent). Library preps were performed using the SMART-Seq v4 Ultra Low Input RNA Kit (Takara Bio) to synthesize full-length cDNA from an input of 10ng of RNA. After a bead-based clean-up to purify the cDNA, the Nextera XT kit was used to create libraries through a process of tagmentation and fragment amplification and appended with dual-indexed bar codes using the NexteraXT DNA Library Preparation kit (Illumina). Libraries were validated by capillary electrophoresis on a Fragment Analyzer (Agilent), pooled at equimolar concentrations, and sequenced on an Illumina NovaSeq6000 (Emory) at 100 bp, paired-end read length targeting ~25 million reads per sample. Repeated measures from a group of PBMC samples collected from healthy controls and repeated measures of a subset of IMPACC samples were used across library prep and sequencing batches to assess inter-site batch effects throughout the study. Universal Human References controls were included to assess intra-site batch variation.

QUANTIFICATION AND STATISTICAL ANALYSIS

Quantification: OMIC-specific processing from raw to computable matrices

Nasal gene expression (NGX)

Base calls were generated in real-time on the NovaSeq6000 instrument (RTA 3.1.5). Demultiplexed, unaligned BAM files were produced by Picard (14) ExtractIlluminaBarcodes, and IlluminaBasecallsToSam were converted to FASTQ format using SamTools bam2fq (15) (v1.4). The sequence read, and base quality were checked using the Trimmomatic-toolkit (16) (v0.36.5). Reads were processed using workflows managed on the Galaxy platform. Reads were trimmed by 1 base at the 3′ end, then trimmed from both ends until base calls had a minimum quality score of at least 30. Any remaining adapter sequence was removed as well. The STAR aligner (17) (v2.4.2a) with the GRCh38 (18) reference genome and gene annotations from Ensembl release 91 (19) was used to align the trimmed reads. Gene counts were generated using HTSeq-count (20) (v0.4.1). Quality metrics were compiled from Picard (v1.134), FASTQC (21) (v0.11.3), Samtools (15) (v1.2), and HTSeq-count (v0.4.1). Failed samples were identified as median cv gene coverage >0.8 and Aligned Counts <1 million. These samples were removed from further downstream analyses.

Serum proteomics targeted (SPT)

Data were analyzed using Real-time PCR analysis software via the ΔΔCt method and Normalized Protein Expression (NPX) manager. NPX is calculated in three steps from the Cq-values: (i) ΔCqsample = Cqsample − Cqextensioncontrol, (ii) ΔΔCq = ΔCqsample − ΔCqinterplatecontrol, (iii) NPX = Correction factor − ΔΔCqsample. Data were normalized using internal controls in every sample, inter-plate control (IPC) and negative controls, and correction factor and expressed as Log2 scale proportional to the protein concentration. One NPX difference equals to the doubling of the protein concentration.

Batch normalization was performed to account for potential batch effects caused by re-assayed samples which were not able to adhere to the study randomization scheme or assay condition changes including those due to assay kit lot# changes or differences in study collection phases. Olink Data Analysis Normalization employed identical reference samples in all plates. NPX value for each analyte was adjusted based on the adjust factor that makes the median of all reference samples the same for all plates. Sequential steps included: 1) the reference sample the-inter-plate-median was calculated; 2) for each assay, the pairwise difference from the inter-plate median was calculated in first step 1 for each of the reference sample on all plates; 3) plate- and assay-specific differences in step 2 were used as normalization factors; and 4) plate- and assay-specific normalization factors were added from step 3 to each value for each assay and plate.

Plasma global proteomics data processing and quality control

All raw timsTOF data were searched on a high-performance computing environment where Fragpipe (including MSFragger, Philosopher, and IonQuant (22–25)) was run to identify and quantify peptides and protein throughout the data (26). MSFragger 3.4 was run using the standard settings without the fixed modification of carboxylmethylation and with the variable modification's oxidation and N-term acetylation. Data were scored against a human FASTA file without isoforms where SARS-COV-2 proteins were manually added. Philosopher 4.1.1 was used where PeptideProphet was used for statistical validation of identified peptides. IonQuant 1.7.17 was used for quantification, where a minimum of 1 ion was used for peptide quantification.

Genes were first filtered based on "Homo Sapiens" and "Homo sapiens OX = 9606". For each sample, the "Total intensity" column was selected. Then Genes without any values across the samples were removed. Finally, sample outliers were removed. A sample is considered an outlier if its total number of quantified proteins is more than 3 standard deviations below the mean of quantified proteins of all samples. In brief, the number of proteins quantified for each sample was calculated, and log2-transformed. Then the mean and standard deviation of quantified proteins across all samples was calculated, and any samples outside 3 standard deviations were considered an outlier and removed. Finally, a protein had to be identified and quantified in at least half of all samples to be analyzed in any of the downstream analyses. We identified 508 proteins that were present in at least 699 (50%) of the samples (out of 2109 proteins in total).

Plasma targeted proteomics data processing

The raw data were exported into Skyline software (27) (v20.2.1.315) for peak area and retention time refinement. The peptide intensity (average of transition pairs) and the protein abundance (average of peptide intensities) in all samples were exported from Skyline. These effects were corrected using Combat (28). The means of the peptide intensities were used for the different protein abundances, which were exported for further analysis using RStudio Pro Server.

Plasma global metabolomics data processing and quality control

Raw data were measured based on LC-MS peak areas proportional to feature concentration. For quality control, missing values were imputed with half the minimum detected level for a given metabolite. Metabolites with an interquartile range of 0 were excluded from the analysis, as previously described (29). All features were log-transformed, normalized then Pareto-scaled to reduce variation in fold-change differences between features (Figures S5A and S5B). After pre-processing, 5 metabolites were filtered out with zero interquartile range, yielding 1012 remaining metabolites (Figure S5C). Statistical analyses for univariate, chemometrics, and clustering analysis used in-house algorithms, R statistical packages, and MetaboAnalyst 5.0 (30, 31).

Blood CyTOF data processing and demultiplexing

Samples from a given batch were acquired on the Fluidigm Helios mass cytometer in multiple acquisitions. The resulting FCS files were normalized and concatenated using Fluidigm's CyTOF software. The FCS file was further cleaned using the Human Immune Monitoring Center at Mt. Sinai's internal pipeline. The pipeline removed any aberrant acquisition time windows of 3 s where the cell sampling event rate was too high or too low (2 standard deviations from the mean). EQ normalization beads that were spiked into every acquisition and used for normalization were removed, along with events that had low DNA signal intensity.

The pipeline was also used to demultiplex the cleaned and pooled FCS files into single sample files. The cosine similarity of every cell's Pd barcoding channels to every possible barcode used in a batch was calculated and then was assigned to its highest similarity barcode. Once the cell had been assigned to a sample barcode, the difference between its highest and second highest similarity scores was calculated and used as a signal-to-noise metric. Any cells with low signal-to-noise were flagged as multiplets and removed from that sample. Finally, acquisition multiplets were removed based on the Gaussian parameters Residual and Offset acquired by the Helios mass cytometer.

Cells from a single biological sample were clustered into 1000 K-means clusters. A subset of samples was then selected and manually annotated into cell types using Clustergrammer2's widget interface (https://github.com/ismms-himc/clustergrammer2) to create a training dataset (n x n matrix of cell types by median marker intensities) for each manually annotated sample.

To annotate a given sample's 1000 K-means clusters, the cosine similarity of every cluster to all possible cell types within the training datasets was calculated, and that cluster was assigned to either its highest similarity score cell type or the greatest consensus cell type across the training datasets. Finally, the cluster cell-type annotation was assigned back to the single cells within that cluster, and the number of cells was calculated for a cell type within a given single sample.

PBMC transcriptomics data processing and quality control

Processing and quality control was performed using an internal Snakemake workflow for RNA-Seq analysis (Github: https://github.com/yerkes-gencore/IMPACC-RNA_Seq). Reads were trimmed for adapter sequence and quality score with cutadapt v1.14112. Reads were aligned with STAR v2.4.2a (17) to a composite reference of human (GRCh38) (18) reference sequence with gene annotations from Ensembl release 91 (19) and SARS-CoV-2 (NCBI strain MN908947.3). Transcript abundance estimates were calculated internal to the STAR aligner using the algorithm of htseq-count94. Sequencing quality metrics were determined using FastQC77 (v0.11.5), alignment quality metrics with Picard tools (v2.22)93 and STAR logs and gene counts, including average quality per read > Q30, percent and absolute counts of reads uniquely mapped to annotated transcripts.

Data preprocessing and additional quality control

Samples included for analysis have undergone prior core internal and assay-specific quality control steps. In addition, proper procedures for quality assurance outlined previously were performed to ensure the data standards for each assay were met. The table below provides information on additional steps to prepare the data for statistical analysis.

Assay name	**Sample filtering**	**Feature filtering**	**Additional batch correction**	**Missing value imputation**	**Data transformation**
PBMC and Nasal gene expression (PGX & NGX)	Passed & questionable QC	Protein coding, genes with CPM >= 1 in >5% of samples in a trajectory group, top 75% highly variable genes	removeBatcheffect from limma	N/A	Scaling
Blood CyTOF	Passed & questionable QC		N/A	N/A	Normalized by total counts per sample with Log1p normalization.
Serum proteomics targeted (SPT)	Passed & questionable QC	N/A	N/A	Impute.knn	Scaling
Plasma proteomics global and targeted (PPG & PPT)	Passed & questionable QC	Removed features with > 30% missing values in training and test sets, separately	N/A	Half-min	Median normalization in linear space, Log2 transformation with pseudocount of 1 and scaling

Plasma metabolomics global (PMG)	Passed & questionable QC	Removed non-xenobiotic features with IQR = 0	N/A	Half-min	Pareto-Scaling

Table S10: Information on data preparation. For each assay, we first filtered out samples using the sample filtering criterion and followed by a filtration on features based on the feature filtering criteria, we performed data imputation and data transformation as indicated in the table. N/A: no additional step taken. Half-min: replacing missing value using half of the minimum of observed values for the corresponding feature. Impute.knn: using impute.knn function from R package impute. Pareto-Scaling: in-house function of dividing each centered variable by the square root of the standard deviation. We evaluated the influence of potential batch effects on different assays using Principal variance component analysis (PVCA) (table S9).

The preprocessing of omic datasets was performed as defined previously (4). These processing steps are briefly described below. Samples with failed or missing QC information were removed for all assays.

Gene expression (PBMC and Nasal) (PGX and NGX)

We filtered for the protein-coding genes and removed lowly expressed genes (genes that do not qualify for counts per million >= 1 in more than 5% of samples in at least one outcome group (trajectory group)). We also removed the 25% least variable gene as evaluated using median absolute deviation (MAD) of log-transformed counts per million values. Finally, we transformed the count data using voom (32), performed batch-correction to remove the effects of technical variables, including phase sample processing batch (phase) and library preparation plates using removeBatchEffect of limma (33), and scaled the data.

Serum proteomics targeted (SPT)

The missing measurements (missing at random) were imputed using nearest neighbor averaging using impute.knn function in R package impute and scaled the data.

Plasma Proteomics (Global and Targeted)

Features with more than 30% missing values separately in training and test sets were removed, and the data was median normalized in linear space, imputed using the half-min approach, log-transformed using pseudocount of 1 and scaled.

Plasma metabolomics global (PMG)

The missing measurements (missing at random) were imputed using the half-min approach, the non-xenobiotic features with IQR = 0 were removed, and pareto-scaled the data.

Whole Blood CyTOF

Cellular population counts were converted to a normalized frequency by dividing by the total counts per sample then log1p transformed. Granulocytes were excluded from the total counts for non-granulocyte populations.

Data imputation via MOFA

Complete assay imputation for the six multi-omic assays (Fig. 1A) was performed using Multi-Omic Factor Analysis (MOFA) via the MOFA2 R package (34, 35). MOFA performs dimensionality reduction through a variational Bayesian framework, modeling high-dimensional multi-omic assays as a product of low-dimensional factor loadings and scores with error, allowing the imputation of entire missing biological assays from the loadings and scores. Imputation was performed on the preprocessed training and test datasets separately to prevent any imputation-wise association between them.

The MOFA model used for imputation featured a large number of factors (200) and had the following summed explained variance per view across all 200 factors: Train - PGX:82.7%, NGX:84.5%, PMG:53.8%, SPT:49.3%, PPG:39.3%, PPT:35.3%. Test - PGX:82.9%, NGX:85.6%, PMG:50.4%, SPT:47.6%, PPG:40.0%, PPT:40.4%.

The effects of MOFA imputation were explored by constructing separate composite regression models for samples missing 0, 1, or 2 assays (fig. S1J). All three models were then tested using the severity task (TG1 vs. TG2/TG3 vs. TG4/TG5) as described in the manuscript and achieved comparable results (fig. S1K).

Multi-omics factor construction via MCIA

Factors were constructed from the preprocessed training multi-omic dataset using Multiple Co-Inertia Analysis (MCIA), which projects data into low-dimensional factors that maximize covariance between each omic and the global data matrix (36). MCIA has shown strong performance in comparison to other unsupervised joint dimensionality reduction methods in multi-omics benchmark comparisons (37, 38). Prior to implementing MCIA, the multi-omics data were standardized using a centered row profile (36), followed by block-level variance normalization (39). Implementation was performed using the mogsa R Bioconductor package (40), with custom modification of the deflation step to constrain global (factor) scores to be orthogonal. MCIA factor scores for preprocessed testing multi-omic samples were calculated by generating block and global scores using coefficients derived from the pretrained MCIA model.

Hierarchical classification model construction and evaluation

Many multi-omic signatures have been found to be associated with disease severity. However, it has also been noticed that mortality sometimes does not lead to immunological variation along the direction of increased severity (41). To capture the signatures indicative of a more severe disease course while accounting for abrupt changes happening for the mortality group, we built a composite prediction model combining a global ordinal regression with a sub-model separating the two most severe groups TG4 and TG5. More specifically, we first fit an ordinal regression model grouping TG4 and TG5 together using the ordinalNet R package (42):

$$P(y \in \cup_{l \geq k} G_l) = \frac{1}{1 + exp\,(-x^\top \beta - \alpha_k)},\ k = 1,2,3$$

where G1= {1}, G2= {2,3}, G3= {4,5}. Then, we further fit a logistic regression model to separate TG4 and TG5 using the glmnet R package (43):

$$P(y = 4) = P(y \in G_3)P(y = 4|y \in G_3) = P(y \in G_3)\frac{1}{1+exp\,(x^{\top}\theta+v)},$$

$$P(y = 5) = P(y \in G_3)P(y = 5|y \in G_3|) = P(y \in G_3)\frac{1}{1+exp\,(-x^{\top}\theta-v)}.$$

Both included Lasso penalties to reduce the influence from nuisance features. The Lasso penalty is tuned using a 10-fold cross-validation, which is recommended to account for both the training efficiency and model variability (44). When compared it to the unstructured multinomial regression model, this structured composite model is more interpretable since the model is characterized by two coefficients: 1) the coefficient 'β' measuring the global trend of being severe, and 2) the coefficient 'θ' identifying the high-risk sub-population among severe patients. Despite being simpler, this composite model provides similar performance to the multinomial logistic regression in our analyses (fig. S1E). Finally, we opted to combine TG2 and TG3 together for both classifiers due to poor performance when separating TG2 from TG3 in the training cohort (AUROC=0.558, fig. S1G).

MCIA model construction and rank selection

Composite regression models were constructed using different ranks of MCIA multi-omic factors from the grid (2, 3, …., 10, 15, 20, 25, 30, 40) using a 50-folds (nested) cross-validation on the training cohort as shown steps 1-2 of the figure below. Minimum deviance loss was achieved for the predictive model with 7 multi-omic MCIA factors (fig. S1F) which we established as the MCIA model. The MCIA model was then used on both the training and testing cohorts to achieve predictions on the testing cohort as shown in step 3 below.

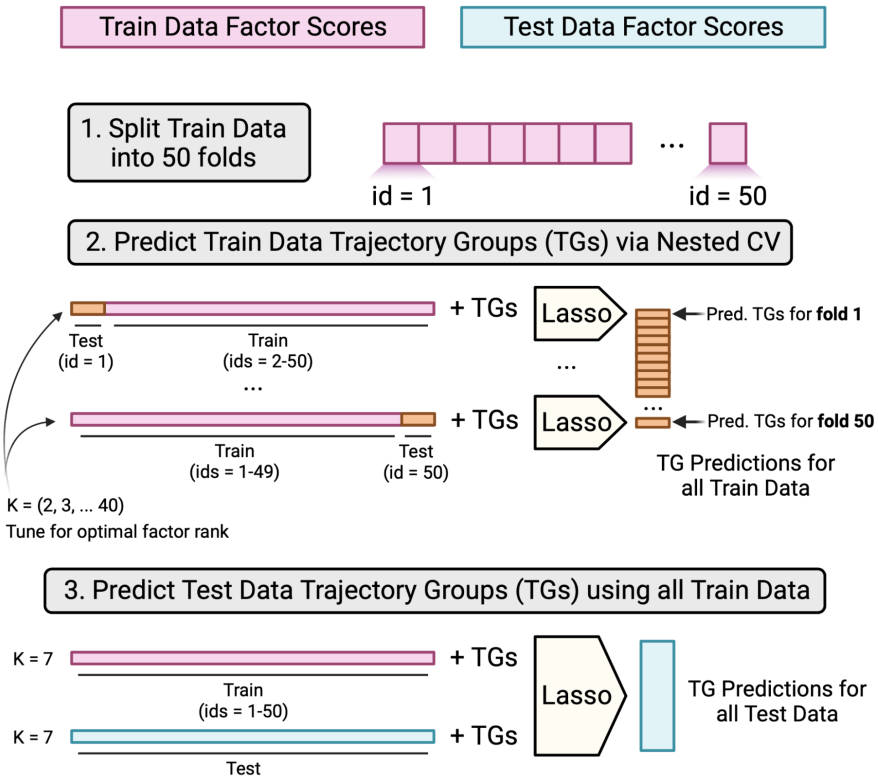

Clinical model construction

A composite regression model utilizing baseline clinical measurements, denoted as the clinical model, was constructed for comparison with the MCIA model. The clinical model features consisted of sex, BMI, age, ethnicity, and race as well as various baseline laboratory values and comorbidities (fig. S1A). We opted to not include the baseline respiratory status into the model as they were utilized in the construction trajectory groups (*5*).

Ensemble (MCIA + clinical) model construction

We considered a simple ensemble of the MCIA model and the clinical model by weighting their predictions where the weights are chosen based on the cross-validation prediction. More specifically, let ${p_i}^{mcia}$ and ${p_i}^{clin}$ denote the prediction of severity (TG4|TG5), we consider the following ensemble prediction for the severity task

$$log\ \frac{{p_i}^{ensemble}}{1-{p_i}^{ensemble}} \leftarrow \alpha_{mcia}\ log\ \frac{{p_i}^{mcia}}{1-{p_i}^{mcia}} + \alpha_{clin}\ log\ \frac{{p_i}^{clin}}{1-{p_i}^{clin}},$$

where α_{mcia} and α_{clin} are chosen by considering an ordinal regression model with response being the TGs and features being log odds of the nested cross-validation prediction version of ${p_i}^{mcia}$ and ${p_i}^{clin}$ on the training cohort.

Similarly, we consider the weighted prediction for the mortality task where the weights are chosen by considering an ordinal regression model with response being the TG5 or TG4 on the among

critical illness, and features being log odds of the nested cross-validation prediction for TG5 in the mortality task.

Model exploration and comparisons via training cohort cross-validation

Both MCIA and ensemble models improved over the clinical model on the training data based on cross-validation (fig. S1B) and conveyed a similar message as the results from the test cohort (Fig. 1C). Additional predictive models were constructed and assessed to the MCIA model (fig. S1, E, H, and I). Groups of constructed models are described below with results sharing the corresponding title. Model performance was measured using both the severity (TG1 vs. TG2/TG3 vs. TG4/TG5) and mortality (TG4 vs. TG5) tasks as described in the manuscript (Fig. 1A).

Multi-omics vs. Single-omics using Concatenation

The MCIA model (MCIA) was compared against the following predictive models: PPT, PPG, SPT, PMG, NGX, and PGX – six separate composite regression models using concatenated analytes from each of the 6 multi-omic assays (without performing dimensionality reduction), All Assays (Concat.) - A composite regression model using all concatenated 27,320 analytes as predictors. MCIA (Multinom.) - A multinomial regression model using the 7 MCIA multi-omics factors rather than the composite classifier framework (fig. S1E).

Multi-omics vs. Single-omics using MCIA

The following models were constructed by using MCIA per-block construction on each assay individually (rather than together): PPT, PPG, SPT, PMG, NGX, and PGX. The MCIA model was shown to emphasize the most predictive assays for each prediction task (fig. S1H).

MCIA Factors vs. Literature

A systematic literature review was performed, searching for biomarkers in the context of COVID-19 severity. Publications were manually assessed for suitability, considering time of biospecimen collection, hospitalization, comparator groups and molecular data types to be as similar to the IMPACC study as possible. Three articles were found as viable candidates, each one containing a molecular signature associated with COVID-19 severity (45–47). Each molecular biomarker was matched to the corresponding IMPACC collected analyte and subsequently utilized to train a separate composite regression model as stated above (fig. S1I).

MCIA separates TG groups with aggregated predictions

To further explore the MCIA model predictions, we combined the results from the severity and mortality tasks to achieve four unique classes: TG1, TG2/TG3, TG4 and TG5. We chose to keep TG2 and TG3 binned together after observing a low AUROC when trying to separate them on the training cohort (fig. S1F). The four classes were utilized in a multi-class AUROC prediction (one versus all) framework. The clinical model was outperformed by the MCIA and ensemble models for every class (fig. S1C).

Finally, we combined the classifier-assigned probabilities from the severity and mortality tasks together to embed participants (fig. S1D). Grouping participants by their TGs revealed a gradual

shift in both the severity (x-axis) and mortality (y-axis) directions, with severity and mortality scores increasing from TG1 < TG2/TG3 < TG4 < TG5.

MCIA predicted risk and hypothesis testing conditional on baseline

To investigate if MCIA model provided additional about clinical trajectory groups conditional on participant's ordinal scale for baseline respiratory, we constructed a predicted severity from the MCIA model and test if the predicted risk is significant in following ordinal regression model:

$$\log P(TG \geq k) = \frac{1}{1+\exp\left(-age*\beta_{age}-sex*\beta_{sex}-baseline*\beta_{base}-risk*\beta_{risk}-\alpha\right)},$$

where "baseline" refers to the score for baseline respiratory status, and "risk" refers to the predicted risk defined as below:

$$predicted\ risk = \sqrt{P(TG = 5) * \ P(TG \in \{4,5\})},$$

which assigns higher risk to patients more likely being in TG4 and TG5 from our MCIA model and shows higher aversion for TG5 compared to TG4. We considered the predicted risk to have significant contribution to the clinical trajectory prediction conditional on the baseline respiratory status if the p-value is smaller than 0.05. We consider this test separately for test-cohort patients with moderately impaired baseline respiratory status (baseline score in [3,4]) and for test-cohort patients with severely impaired baseline respiratory status (baseline score in [5,6]) to examine if the predicted risk if conditionally informative about future clinical trajectory given different incoming status.

Baseline and longitudinal differential analysis of factors

We performed a cumulative link mixed effect analysis using MCIA factor scores from baseline samples and investigated (1) if there is an ordinal trend from TG1 to TG5 and (2) if any pair of groups exhibit significant differences. Enrollment sites were assigned as a random effect and age group (split across five quantiles ([18,35], [36,51], [52,66], [67,81], [82,96])) and sex were included as fixed effects. We tested for the ordinal trend with the clmm function from the R package ordinal (48) (v 2019.12-10) and pairwise difference with the lmer function from the R package lme4 (49) (v 1.1-27.1). We identified significant MCIA factors whose adjusted p values (Benjamini-Hochberg Procedure (50)) are below 0.05 for the ordinal trend or for the pairwise comparisons between TG4 and TG5. Significant factors can potentially be used for separating clinical groups at hospital admission.

We next moved to longitudinal analysis for scheduled visits (Visits 1-6) to identify MCIA factors whose scores differ for different clinical groups from the training set ranging from day 0 (admission) to day 41. We performed a linear mixed modeling analysis for the factor levels using the lme function from the R package nlme (51) (v 3.1-148) and a mixed generalized additive modeling analysis and modeled the factor levels as a smooth function (cubic regression) of admission time using the R package gamm4 (52) (v 0.2-6) function gamm4. For each pair of groups, we tested if the two groups have different longitudinal trends for the MCIA factors after including the participant ID and enrollment site as random effects while sex and age group as fixed effects. We claimed significance when the adjusted p-value is below 0.05, and significant factors could indicate interesting molecular dynamics across clinical groups:

factor ~ s(admission date, bs = cr) + s(admission date, bs = cr, by =TG) + TG + sex + age+ (1|enrollment_site/participant id).

Here, s(., bs=cr) indicates we are using a smooth spline to model the overall kinetics over admission dates, for pooled participants and each TG group (by=TG), and the term (1|enrollment site/participant id) indicates a nested random effect by participant id and enrollment site.a

The testing results for baseline (visit) and longitudinal analysis for 7 selected factors are shown in table s4.

Definition of high-contribution features

The MCIA dimension reduction uses all features in its multi-omics factor construction. To identify the top contributing features associated with each MCIA multi-omics factor, we defined high-contribution features for each assay as the features whose absolute factor weights >=0.2 and Benjamini-Hochberg adjusted p-values for correlation with a factor satisfying p.adj <= 0.01.

Factor annotation and enrichment analysis

Databases: Publicly available knowledge databases were used for functional enrichment analysis, with details listed below.

- KEGG: A list of KEGG pathways and their corresponding mappings with genes and metabolites were extracted using the KEGG REST API (Release 102.0). KEGG pathways were used for gene/protein/metabolite annotations.
- Hallmark: Hallmark pathways are extracted from MsigDB database (Homo sapien) using msigdbr (version 7.5.1). Hallmark pathways were used for gene and protein annotations.
- Subpathway: Many metabolites in the plasma global metabolomics lack KEGG id correspondence. Hence, when we encountered difficulty using KEGG pathways, we used the subpathway database provided by Metabolon for metabolite annotation (9, 53, 54).
- Immunoglobulin gene sets: The GO terms with “IMMUNOGLOBULIN” in the name were extracted from MSigDB (c5 v7.5.1)
- C3 was extracted from MSigDB (C3 v7.5.1): for transcription factor and miRNA gene sets functional enrichment.
- Ligand-receptor signaling-based gene sets were constructed from the ligand/receptor and intracellular signaling reported in Omnipath, with ligand’s gene sets being composed of all genes within one connection of their receptors.
- A list of IFN inhibitors was extracted from *Porritt and Herzog* (55) for enrichment and generation of composite scores of these genes for baseline and longitudinal analysis.

Enrichment analysis using high-contribution features with mHG:

Enrichment analyses were conducted on the MCIA predictive model trained using the initial 539 participants and validated on the remaining 613 participants. Enrichment of the factors was conducted using the minimum hypergeometric test (mHG) from the R package mHG (56) (v 1.1) using the gene, proteins and metabolite sets from the Hallmark, KEGG (downloaded on August 04, 2022), and C3 on high-contribution features of a factor. The joint p-value combines enrichment p-values from assays which contained non-zero features in each pathway using the Cauchy

combination test, which is known to be robust to the dependence structure underlying p-values to be combined (57). The selection of an appropriate background set of features is crucial for the accurate enrichment analysis. We used only those features as background that were measured in our assays. Since the serum Olink (SPT) included only 92 proteins in total, which were preselected for their function in inflammation, the enrichment over the background of 92 features did not yield many significant pathways as expected. Therefore, to capture meaningful signal from the SPT, we also performed a direct comparison of the SPT features with features and pathways of other datasets using an 'inter-omics association analysis' (see below).

Selection of enriched pathways of severity factor for further consideration

The pathway databases are comprised of many broad and redundant biological pathways with highly overlapping genesets (58). We obtained significant enrichment for a large number of pathways, many of which represented redundant biological function. To handle this redundancy, we first collected biological pathways that were significantly enriched (adj.p<0.1) in each assay in the severity factor, and we clustered them based on the number of shared leading-edge features and visualized using enrichment map plot (fig. S2A). We observed main four major functional categories: inflammation, T-cell activity, cell death, and dysregulated metabolism of essential amino acids (fig. S2, A and B, table s5). We prioritized the pathways based on the strongest joint p-values (as described above) and selected the representative pathways from each of the four functional categories that reflected specialized biological functions and displayed most significant aggregated p-values. We favored the pathways with significant enrichment in at least two omics as representatives from each functional category, except for "Th1 and Th2 cell differentiation" and "T-cell receptor signaling pathway" in T-cell activity and "Tryptophan metabolism" in dysregulated metabolism categories. (Fig 3C), because the features of some of these pathways are not expected to be highly represented in other datasets, for example, metabolic features are present only in PMG and the genes encoding the enzymes involved in those metabolic pathways are not very well defined in existing knowledge bases. Similarly, TCR-signaling genes are expected to be enriched in the gene expression datasets compared to the plasma/serum proteomics datasets.

For the pathways enriched in the mortality factor, we further selected only those pathways that separated TG4 and TG5 at baseline because the dominant signal that the mortality factor captures is related to the separation of these two groups at baseline (table s7 for all enriched pathways and table s8 for pathways that show separation between TG4 and TG5, p.val < 0.05). Transcriptomics pathways including Influenza A, Epstein-Barr virus infection, Hepatitis C, Measles and Herpes simplex virus 1 infection are subsets of the listed interferon signaling pathways shown in Fig. 5C, hence omitted from the main Figure.

TG4|5 filtered enrichment:

The mHG test allows for flexible filtering of the ordered feature list before passing to the MHG test function. Apart from the plain enrichment analysis, we further considered a TG4|5 filtered enrichment analysis for each factor where we kept only high-contribution metabolites and soluble proteins who can separate TG4 and TG5 at baseline (training samples only) with p.val <=0.05 and performed MHG test using the filtered list (table s6 and table s8). This helped us avoid

overlooking important functions related to the early separation of TG4 and TG5 due to the overwhelming signals from temporal kinetics and related to the overall disease severity (from TG1 to TG5).

Cell-type enrichment analysis via GSEA:

Due to the limited size of overlaps between cell markers and high-contribution feature, Gene Set Enrichment Analysis (GSEA) for cell type enrichment of the PBMC and nasal transcriptomics was conducted using gene sets from Nakaya H. et al. (59) and a combined gene set of Ziegler et al. (60) with the neutrophil and eosinophil marker genes from Ordovas-Montanes et al. (61) respectively.

Pathway activity construction

The pathway activities were calculated as a weighted sum of selected features of a pathway. Specifically, for pathways included in the enrichment analysis, we identified the features that contributed to the enrichment of the pathway, also known as the leading-edge features. We multiplied the levels of each leading-edge feature with its absolute factor weight in the factor and calculated a sum of the weighted levels across the features as pathway activity. For an unbiased evaluation of the NGX IFN inhibitory genes and NGX Hallmark IFN Alpha Response in Fig. 6, the pathway activities were instead calculated and modeled as the average of all detected features in the gene sets.

Detailed evaluations of pathway activities

For pathways of interest, we performed mixed generalized additive modeling analysis and modeled the pathway activity as a smooth function of admission time using the R package gamm4 (52) (v 0.2-6) function gamm4. We included participant ID and enrollment site as random effects while sex and age quintile as fixed effects, as we have done in the factor longitudinal test:

pathway_activity ~ s(admission date, bs = cr) + s(admission date, bs = cr, by =TG) + TG + sex + age+(1|enrollment site/participant id)

For the T cell pathway analysis in Fig. S3C, we calculated a sum of PBMC transcriptomic levels of all features in the indicated KEGG pathway and used our longitudinal modal analysis (as described above) while using T cell frequencies measured in whole blood CyTOF (combined across all T cell subsets) as a covariate to adjust for the cell abundance changes:

pathway_activity ~ s(admission date, bs = cr) + s(admission date, bs = cr, by =TG) + TG + sex + age+ CD4+T cell frequency + CD8+T cell frequency+(1|enrollment site/participant id)

Inter-omics association analysis

The inter-omics associations test for identifying strong connections between two different omics used the Pearson correlation test after adjusting for age, sex, enrollment site. In addition, we further adjusted visit numbers and clinical trajectory groups to account for the global co-varying patterns and the feature selection effects as we investigated the inter-omics associations among high-contribution features. We used a stringent cutoff to identify the strongest associations between assays using the Bonferroni correction to control the family wise error rate (FWER) with

adj.p<0.01. The p-value for covariates-adjusted association was calculated using a linear mixed-effect modeling where we also included random effects at the participant level to account for spurious correlation caused for correlated noise for samples from the same participant.

Although each factor captures co-varying patterns across omics, the factor represents global systematic changes, and does not directly guarantee local connections between a pair of high-contribution features. Additionally, the factors do not provide direct connection of individual features to biological pathways (combined expression signatures over multiple genes/proteins). We performed inter-omics association analysis to investigate the local connections between immune components from different assays. The inter-omics analysis not only assesses the direct association between two analytes or pathway functions, but it also helps to capture meaningful functional descriptions additional to the enrichment test, by linking SPT analytes directly to enriched pathways from other assays. We consider the associations between the following types (fig. S4, fig. S6C):

1. Task 1: Association between plasma metabolite pathway activities and serum targeted proteomics. Association between metabolite pathway activities and plasma protein/gene pathway activities (both nasal and PBMC).
2. Task 2: Association between serum targeted proteomics and plasma protein/gene pathway activities (both nasal and PBMC).
3. Task 3: Association between plasma metabolite pathway activities and plasma protein/gene pathway activities (both nasal and PBMC).
4. Task 4: Association between metabolite pathway activities/ serum targeted proteomics and whole blood cell frequencies (parent population) measured by CyTOF.

We performed Tasks 1-4 for high-contribution cytokines and highlighted pathways activities for each factor. We summarized assay variability captured by a factor for assays other than serum targeted proteomics (Olink) using pathway activities because they were of high dimensions and individual features revealed less-interpretable information than the pathway activity. Exact formulas for calculating covariates-adjusted Pearson correlation and p-values from mixed effect modeling are given below.

Tasks 1-3 (inter-omics associations among primary assays used in MCIA factors).

P-value calculation: We further adjust for the visit numbers and TG assignments to alleviate the co-selection effects of high-contribution features, and consider the formula: Omic feature1 ~ Omic feature 2 + sex+age+visit_number+TG+(1|enrollment site/participant id).

Correlation calculation: Pearson correlations between the residual of an omic feature and the residual of another omic feature after regressing out age, sex, and enrollment site, visit numbers and TG groups.

Task 4 (inter-omics associations with CyToF cell frequencies)

P-value calculation: we consider Omic feature ~ cell frequency + Omic feature ~ cell frequency + sex + age + (1|enrollment site/participant id), where (1|enrollment site/participant id) indicates a nested random effect by participant id and enrollment site.

Correlation calculation: Pearson correlations between the residual of an omic feature and the residual of a cell frequency after regressing out age, sex, and enrollment site.

Viral-adjusted IFN signaling analysis

To understand the influence of viral loads in the IFN signaling differences observed comparing TG4 and TG5, we conducted a viral-adjusted IFN signaling analysis. Since the interaction between viral loads and IFN signaling are highly non-linear, we adjust for viral loads using random forest to avoid subjective transformation.

1. Baseline comparison: We fitted a random forest model predicting baseline IFN signaling pathway levels from baseline viral loads (default parameter, keeping samples where both viral loads nasal transcriptomics and viral loads measurements), and the fitted residuals were used Wilcoxon test for comparing TG4 and TG5 and moderate illness (TG1/TG2/TG3) vs. critical illness (TG4/TG5).
2. Kinetics comparison: We fitted a random forest model predicting IFN signaling pathway levels from viral loads using all samples (default parameter, keeping samples where both viral loads nasal transcriptomics and viral loads measurements were available), and the fitted residuals were used for comparing the kinetics from TG4 and TG5 (gamm4, mixed effect modeling where participant id is modeled as the random effect).

The viral adjusted results were compared to the unadjusted results. For a fair comparison, in this analysis alone, we used the same set of samples for the unadjusted/adjusted tests where both nasal transcriptomics and viral loads were available.

References:

1. Ozonoff A, et al. Phenotypes of disease severity in a cohort of hospitalized COVID-19 patients: Results from the IMPACC study. *eBioMedicine*. 2022;83:104208.
2. IMPACC Manuscript Writing Team, IMPACC Network Steering Committee. Immunophenotyping assessment in a COVID-19 cohort (IMPACC): A prospective longitudinal study. *Sci Immunol*. 2021;6(62):eabf3733.
3. Beigel JH, et al. Remdesivir for the Treatment of Covid-19 - Final Report. *N Engl J Med*. 2020;383(19):1813–1826.
4. Diray-Arce J, et al. Multi-omic longitudinal study reveals immune correlates of clinical course among hospitalized COVID-19 patients. *Cell Rep Med*. 2023;4(6):101079.
5. Carreño JM, et al. Activity of convalescent and vaccine serum against SARS-CoV-2 Omicron. *Nature*. 2022;602(7898):682–688.
6. Carreño JM, et al. Evidence for retained spike-binding and neutralizing activity against emerging SARS-CoV-2 variants in serum of COVID-19 mRNA vaccine recipients. *EBioMedicine*. 2021;73:103626.
7. Viodé A, et al. Plasma Proteomic Analysis Distinguishes Severity Outcomes of Human Ebola Virus Disease. *mBio*. 2022;13(3):e0056722.
8. Hughes CS, et al. Single-pot, solid-phase-enhanced sample preparation for proteomics experiments. *Nat Protoc*. 2019;14(1):68–85.

9. Evans AM, et al. Integrated, nontargeted ultrahigh performance liquid chromatography/electrospray ionization tandem mass spectrometry platform for the identification and relative quantification of the small-molecule complement of biological systems. *Anal Chem*. 2009;81(16):6656–6667.
10. Long T, et al. Whole-genome sequencing identifies common-to-rare variants associated with human blood metabolites. *Nat Genet*. 2017;49(4):568–578.
11. Spicer RA, Salek R, Steinbeck C. A decade after the metabolomics standards initiative it's time for a revision. *Sci Data*. 2017;4:170138.
12. Sumner LW, et al. Proposed minimum reporting standards for chemical analysis Chemical Analysis Working Group (CAWG) Metabolomics Standards Initiative (MSI). *Metabolomics*. 2007;3(3):211–221.
13. MSI Board Members, et al. The metabolomics standards initiative. *Nat Biotechnol*. 2007;25(8):846–848.
14. Picard Toolkit. 2019. https://broadinstitute.github.io/picard/.
15. Li H, et al. The Sequence Alignment/Map format and SAMtools. *Bioinformatics*. 2009;25(16):2078–2079.
16. Bolger AM, Lohse M, Usadel B. Trimmomatic: a flexible trimmer for Illumina sequence data. *Bioinformatics*. 2014;30(15):2114–2120.
17. Dobin A, et al. STAR: ultrafast universal RNA-seq aligner. *Bioinformatics*. 2013;29(1):15–21.
18. Schneider VA, et al. Evaluation of GRCh38 and de novo haploid genome assemblies demonstrates the enduring quality of the reference assembly. *Genome Res*. 2017;27(5):849–864.
19. Cunningham F, et al. Ensembl 2019. *Nucleic Acids Research*. 2019;47(D1):D745–D751.
20. Anders S, Pyl PT, Huber W. HTSeq—a Python framework to work with high-throughput sequencing data. *Bioinformatics*. 2015;31(2):166–169.
21. Andrews, S. FastQC: A Quality Control Tool for High Throughput Sequence Data. 2010. http://www.bioinformatics.babraham.ac.uk/projects/fastqc.
22. Yu F, Haynes SE, Nesvizhskii AI. IonQuant Enables Accurate and Sensitive Label-Free Quantification With FDR-Controlled Match-Between-Runs. *Molecular & Cellular Proteomics*. 2021;20:100077.
23. da Veiga Leprevost F, et al. Philosopher: a versatile toolkit for shotgun proteomics data analysis. *Nat Methods*. 2020;17(9):869–870.
24. Kong AT, et al. MSFragger: ultrafast and comprehensive peptide identification in mass spectrometry–based proteomics. *Nat Methods*. 2017;14(5):513–520.
25. Yu F, et al. Fast Quantitative Analysis of timsTOF PASEF Data with MSFragger and IonQuant. *Mol Cell Proteomics*. 2020;19(9):1575–1585.
26. van Zalm P, et al. A Parallelization Strategy for the Time Efficient Analysis of Thousands of LC/MS Runs in High-Performance Computing Environment. *J Proteome Res*. 2022;21(11):2810–2814.
27. MacLean B, et al. Skyline: an open source document editor for creating and analyzing targeted proteomics experiments. *Bioinformatics*. 2010;26(7):966–968.
28. Johnson WE, Li C, Rabinovic A. Adjusting batch effects in microarray expression data using empirical Bayes methods. *Biostatistics*. 2007;8(1):118–127.
29. Diray-Arce J, et al. Bacille Calmette-Guérin vaccine reprograms human neonatal lipid metabolism in vivo and in vitro. *Cell Rep*. 2022;39(5):110772.

30. Pang Z, et al. MetaboAnalyst 5.0: narrowing the gap between raw spectra and functional insights. *Nucleic Acids Research*. 2021;49(W1):W388–W396.
31. Xia J, Wishart DS. Metabolomic Data Processing, Analysis, and Interpretation Using MetaboAnalyst. *Current Protocols in Bioinformatics*. 2011;34(1):14.10.1-14.10.48.
32. Law CW, et al. voom: Precision weights unlock linear model analysis tools for RNA-seq read counts. *Genome Biol*. 2014;15(2):R29.
33. Ritchie ME, et al. limma powers differential expression analyses for RNA-sequencing and microarray studies. *Nucleic Acids Res*. 2015;43(7):e47.
34. Argelaguet R, et al. Multi-Omics Factor Analysis-a framework for unsupervised integration of multi-omics data sets. *Mol Syst Biol*. 2018;14(6):e8124.
35. Argelaguet R, et al. MOFA+: a statistical framework for comprehensive integration of multi-modal single-cell data. *Genome Biol*. 2020;21(1):111.
36. Meng C, et al. A multivariate approach to the integration of multi-omics datasets. *BMC Bioinformatics*. 2014;15:162.
37. Tini G, et al. Multi-omics integration-a comparison of unsupervised clustering methodologies. *Brief Bioinform*. 2019;20(4):1269–1279.
38. Cantini L, et al. Benchmarking joint multi-omics dimensionality reduction approaches for the study of cancer. *Nat Commun*. 2021;12(1):124.
39. Abdi H, et al. STATIS and DISTATIS: optimum multitable principal component analysis and three way metric multidimensional scaling. *WIREs Computational Statistics*. 2012;4(2):124–167.
40. Meng C, et al. MOGSA: Integrative Single Sample Gene-set Analysis of Multiple Omics Data. *Mol Cell Proteomics*. 2019;18(8 suppl 1):S153–S168.
41. Lucas C, et al. Longitudinal analyses reveal immunological misfiring in severe COVID-19. *Nature*. 2020;584(7821):463–469.
42. Wurm MJ, Rathouz PJ, Hanlon BM. Regularized Ordinal Regression and the ordinalNet R Package. *J Stat Softw*. 2021;99(6). https://doi.org/10.18637/jss.v099.i06.
43. Friedman JH, Hastie T, Tibshirani R. Regularization Paths for Generalized Linear Models via Coordinate Descent. *Journal of Statistical Software*. 2010;33:1–22.
44. Hastie T, Tibshirani, R., Friedman, J. *The elements of statistical learning: data mining, inference, and prediction*. New York: Springer; .
45. Gisby J, et al. Longitudinal proteomic profiling of dialysis patients with COVID-19 reveals markers of severity and predictors of death. *Elife*. 2021;10:e64827.
46. Ling L, et al. Longitudinal Cytokine Profile in Patients With Mild to Critical COVID-19. *Front Immunol*. 2021;12:763292.
47. Patterson BK, et al. Immune-Based Prediction of COVID-19 Severity and Chronicity Decoded Using Machine Learning. *Front Immunol*. 2021;12:700782.
48. Christensen RHB. ordinal—Regression Models for Ordinal Data. https://CRAN.R-project.org/package=ordinal.
49. Bates D, et al. Fitting Linear Mixed-Effects Models Using lme4. *Journal of Statistical Software*. 2015;67:1–48.
50. Benjamini Y, Hochberg Y. Controlling the False Discovery Rate: A Practical and Powerful Approach to Multiple Testing. *Journal of the Royal Statistical Society Series B (Methodological)*. 1995;57(1):289–300.
51. Jose C. Pinheiro, Douglas M. Bates. *Mixed-Effects Models in S and S-PLUS*. New York: Springer; .

52. Simon Wood, Fabian Scheipl. gamm4: Generalized Additive Mixed Models using “mgcv” and “lme4.”
53. Evans AM, et al. Dissemination and analysis of the quality assurance (QA) and quality control (QC) practices of LC-MS based untargeted metabolomics practitioners. *Metabolomics*. 2020;16(10):113.
54. Dehaven CD, et al. Organization of GC/MS and LC/MS metabolomics data into chemical libraries. *J Cheminform*. 2010;2(1):9.
55. Porritt RA, Hertzog PJ. Dynamic control of type I IFN signalling by an integrated network of negative regulators. *Trends Immunol*. 2015;36(3):150–160.
56. Perl K. mHG: Minimum-Hypergeometric test. 2015.
57. Liu Y, Xie J. Cauchy combination test: a powerful test with analytic p-value calculation under arbitrary dependency structures. *J Am Stat Assoc*. 2020;115(529):393–402.
58. Vivar JC, et al. Redundancy control in pathway databases (ReCiPa): an application for improving gene-set enrichment analysis in Omics studies and “Big data” biology. *OMICS*. 2013;17(8):414–422.
59. Nakaya HI, et al. Systems biology of vaccination for seasonal influenza in humans. *Nat Immunol*. 2011;12(8):786–795.
60. Ziegler CGK, et al. Impaired local intrinsic immunity to SARS-CoV-2 infection in severe COVID-19. *Cell*. 2021;184(18):4713-4733.e22.
61. Ordovas-Montanes J, et al. Allergic inflammatory memory in human respiratory epithelial progenitor cells. *Nature*. 2018;560(7720):649–654.

[#]**The IMPACC Network**

National Institute of Allergy and Infectious Diseases, National Institute of Health, Bethesda, MD 20814, USA: Patrice M. Becker, Alison D. Augustine, Steven M. Holland, Lindsey B. Rosen, Serena Lee, Tatyana Vaysman

Clinical and Data Coordinating Center (CDCC) Precision Vaccines Program, Boston Children's Hospital, Boston, MA 02115, USA: Al Ozonoff, Joann Diray-Arce, Jing Chen, Alvin Kho, Carly E. Milliren, Annmarie Hoch, Ana C. Chang, Kerry McEnaney, Brenda Barton, Claudia Lentucci, Maimouna D. Murphy, Mehmet Saluvan, Tanzia Shaheen, Shanshan Liu, Caitlin Syphurs, Marisa Albert, Arash Nemati Hayati, Robert Bryant, James Abraham, Sanya Thomas, Mitchell Cooney

Benaroya Research Institute, University of Washington, Seattle, WA 98101, USA: Matthew C. Altman, Naresh Doni Jayavelu, Scott Presnell, Bernard Kohr, Tomasz Jancsyk, Azlann Arnett

La Jolla Institute for Immunology, La Jolla, CA 92037, USA: Bjoern Peters, James A. Overton, Randi Vita, Kerstin Westendorf

Knocean Inc. Toronto, ON M6P 2T3, Canada: James A. Overton

Precision Vaccines Program, Boston Children's Hospital, Harvard Medical School, Boston, MA 02115, USA: Ofer Levy, Hanno Steen, Patrick van Zalm, Benoit Fatou, Kinga Smolen, Arthur Viode, Simon van Haren, Meenakshi Jha, David Stevenson

Brigham and Women's Hospital, Harvard Medical School, Boston, MA 02115, USA: Lindsey R. Baden, Kevin Mendez, Jessica Lasky-Su, Alexandra Tong, Rebecca Rooks, Michael Desjardins, Amy C. Sherman, Stephen R. Walsh, Xhoi Mitre, Jessica Cauley, Xiofang Li, Bethany Evans, Christina Montesano, Jose Humberto Licona, Jonathan Krauss, Nicholas C. Issa, Jun Bai Park Chang, Natalie Izaguirre

Metabolon Inc, Morrisville, NC 27560, USA: Scott R. Hutton, Greg Michelotti, Kari Wong

Prevention of Organ Failure (PROOF) Centre of Excellence, University of British Columbia, Vancouver, BC V6T 1Z3, Canada: Scott J. Tebbutt, Casey P. Shannon

Case Western Reserve University and University Hospitals of Cleveland, Cleveland, OH 44106, USA: Rafick-Pierre Sekaly, Slim Fourati, Grace A. McComsey, Paul Harris, Scott Sieg, Susan Pereira Ribeiro

Drexel University, Tower Health Hospital, Philadelphia, PA 19104, USA: Charles B. Cairns, Elias K. Haddad, Michele A. Kutzler, Mariana Bernui, Gina Cusimano, Jennifer Connors, Kyra Woloszczuk, David Joyner, Carolyn Edwards, Edward Lee, Edward Lin, Nataliya Melnyk, Debra L. Powell, James N. Kim, I. Michael Goonewardene, Brent Simmons, Cecilia M. Smith, Mark Martens, Brett Croen, Nicholas C. Semenza, Mathew R. Bell, Sara Furukawa, Renee McLin, George P. Tegos, Brandon Rogowski, Nathan Mege, Kristen Ulring, Pam Schearer, Judie Sheidy, Crystal Nagle

MyOwnMed Inc., Bethesda, MD 20817, USA: Vicki Seyfert-Margolis

Emory School of Medicine, Atlanta, GA 30322, USA: Nadine Rouphael, Steven E. Bosinger, Arun K. Boddapati, Greg K. Tharp, Kathryn L. Pellegrini, Brandi Johnson, Bernadine Panganiban, Christopher Huerta, Evan J. Anderson, Hady Samaha, Jonathan E. Sevransky, Laurel Bristow, Elizabeth Beagle, David Cowan, Sydney Hamilton, Thomas Hodder, Amer Bechnak, Andrew Cheng, Aneesh Mehta, Caroline R. Ciric, Christine Spainhour, Erin Carter, Erin M. Scherer, Jacob Usher, Kieffer Hellmeister, Laila Hussaini, Lauren Hewitt, Nina Mcnair, Susan Pereira Ribeiro

Icahn School of Medicine at Mount Sinai, New York, NY 10029, USA: Ana Fernandez-Sesma, Viviana Simon, Florian Krammer, Harm Van Bakel, Seunghee Kim-Schulze, Ana Silvia Gonzalez-Reiche, Jingjing Qi, Brian Lee, Juan Manuel Carreño, Gagandeep Singh, Ariel Raskin, Johnstone Tcheou, Zain Khalil, Adriana van de Guchte, Keith Farrugia, Zenab Khan, Geoffrey Kelly, Komal Srivastava, Lily Q. Eaker, Maria C. Bermúdez-González, Lubbertus C.F. Mulder, Katherine F. Beach, Miti Saksena, Deena Altman, Erna Kojic, Levy A. Sominsky, Arman Azad, Dominika Bielak, Hisaaki Kawabata, Temima Yellin, Miriam Fried, Leeba Sullivan, Sara Morris, Giulio Kleiner, Daniel Stadlbauer, Jayeeta Dutta, Hui Xie, Manishkumar Patel, Kai Nie

Immunai Inc. New York, NY 10016, USA: Adeeb Rahman

Oregon Health Sciences University, Portland, OR 97239, USA: William B. Messer, Catherine L. Hough, Sarah A.R. Siegel, Peter E. Sullivan, Zhengchun Lu, Amanda E. Brunton, Matthew Strnad, Zoe L. Lyski, Felicity J. Coulter, Courtney Micheleti

Stanford University School of Medicine, Palo Alto, CA 94305, USA: Holden Maecker, Bali Pulendran, Kari C. Nadeau, Yael Rosenberg-Hasson, Michael Leipold, Natalia Sigal, Angela Rogers, Andrea Fernandes, Monali Manohar, Evan Do, Iris Chang, Alexandra S. Lee, Catherine Blish, Henna Naz Din, Jonasel Roque, Linda Geng, Maja Artandi, Mark M. Davis, Neera Ahuja, Samuel S. Yang, Sharon Chinthrajah, Thomas Hagan

David Geffen School of Medicine at the University of California Los Angeles, Los Angeles CA 90095, USA: Elaine F. Reed, Joanna Schaenman, Ramin Salehi-Rad, Adreanne M. Rivera, Harry C. Pickering, Subha Sen, David Elashoff, Dawn C. Ward, Jenny Brook, Estefania Ramires-Sanchez, Megan Llamas, Claudia Perdomo, Clara E. Magyar, Jennifer Fulcher

University of California San Francisco, San Francisco, CA 94115, USA: David J. Erle, Carolyn S. Calfee, Carolyn M. Hendrickson, Kirsten N. Kangelaris, Viet Nguyen, Deanna Lee, Suzanna Chak, Rajani Ghale, Ana Gonzalez, Alejandra Jauregui, Carolyn Leroux, Luz Torres Altamirano, Ahmad Sadeed Rashid, Andrew Willmore, Prescott G. Woodruff, Matthew F. Krummel, Sidney Carrillo, Alyssa Ward, Charles R. Langelier, Ravi Patel, Michael Wilson, Ravi Dandekar, Bonny Alvarenga, Jayant Rajan, Walter Eckalbar, Andrew W. Schroeder, Gabriela K. Fragiadakis, Alexandra Tsitsiklis, Eran Mick, Yanedth Sanchez Guerrero, Christina Love, Lenka Maliskova, Michael Adkisson, Aleksandra Leligdowicz, Alexander Beagle, Arjun Rao, Austin Sigman, Bushra Samad, Cindy Curiel, Cole Shaw, Gayelan Tietje-Ulrich, Jeff Milush, Jonathan Singer, Joshua J. Vasquez, Kevin Tang, Legna Betancourt, Lekshmi Santhosh, Logan Pierce, Maria Tecero Paz, Michael Matthay, Neeta Thakur, Nicklaus Rodriguez, Nicole Sutter, Norman Jones, Pratik Sinha, Priya Prasad, Raphael Lota, Sadeed Rashid, Saurabh Asthana, Sharvari Bhide, Tasha Lea, Yumiko Abe-Jones

Yale School of Medicine, New Haven, CT 06510, USA: David A. Hafler, Ruth R. Montgomery, Albert C. Shaw, Steven H. Kleinstein, Jeremy P. Gygi, Shrikant Pawar, Anna Konstorum, Ernie Chen, Chris Cotsapas, Xiaomei Wang, Leqi Xu, Charles Dela Cruz, Akiko Iwasaki, Subhasis

Mohanty, Allison Nelson, Yujiao Zhao, Shelli Farhadian, Hiromitsu Asashima, Omkar Chaudhary, Andreas Coppi, John Fournier, Khadir Raddassi, Michael Rainone, William Ruff, Syim Salahuddin, Wade L. Schulz, Pavithra Vijayakumar, Haowei Wang, H. Patrick Young

Yale School of Public Health, New Haven, CT 06510, USA: Denise Esserman, Leying Guan, Anderson Brito, Jessica Rothman, Nathan D. Grubaugh, Elsio Wunder Jr., Catherine Muenker, Albert I. Ko

Baylor College of Medicine and the Center for Translational Research on Inflammatory Diseases, Houston, TX 77030, USA: David B. Corry, Farrah Kheradmand, Li-Zhen Song, Ebony Nelson

Oklahoma University Health Sciences Center, Oklahoma City, OK 73104, USA: Jordan P. Metcalf, Nelson I. Agudelo Higuita, Lauren A. Sinko, J. Leland Booth, Douglas A. Drevets, Brent R. Brown

University of Arizona, Tucson AZ 85721, USA: Monica Kraft, Chris Bime, Jarrod Mosier, Heidi Erickson, Ron Schunk, Hiroki Kimura, Michelle Conway, Dave Francisco, Allyson Molzahn, Connie Cathleen Wilson, Ron Schunk, Trina Hughes, Bianca Sierra

University of Florida, Gainesville, FL 32611, USA: Mark A. Atkinson, Scott C. Brakenridge, Ricardo F. Ungaro, Brittany Roth Manning, Lyle Moldawer

University of Florida, Jacksonville, FL 32218, USA: Jordan Oberhaus, Faheem W. Guirgis

University of South Florida, Tampa FL 33620, USA: Brittney Borresen, Matthew L. Anderson

University of Texas, Austin, TX 78712, USA: Lauren I. R. Ehrlich, Esther Melamed, Cole Maguire, Dennis Wylie, Justin F. Rousseau, Kerin C. Hurley, Janelle N. Geltman, Nadia Siles, Jacob E. Rogers.

IMPACC Network Competing Interests

The Icahn School of Medicine at Mount Sinai has filed patent applications relating to SARS-CoV-2 serological assays and NDV-based SARS-CoV-2 vaccines which list Florian Krammer as co-inventor. Mount Sinai has spun out a company, Kantaro, to market serological tests for SARS-CoV-2. Florian Krammer has consulted for Merck and Pfizer (before 2020), and is currently consulting for Pfizer, Seqirus, 3rd Rock Ventures, Merck and Avimex. The Krammer laboratory is also collaborating with Pfizer on animal models of SARS-CoV-2. Viviana Simon is a co-inventor on a patent filed relating to SARS-CoV-2 serological assays (the "Serology Assays"). Ofer Levy is a named inventor on patents held by Boston Children's Hospital relating to vaccine adjuvants and human in vitro platforms that model vaccine action. He is a cofounder of Ovax, Inc, has consulted for GlaxoSmithKline (GSK) and Hillevax and leads a laboratory that has received research support from GSK. Charles Cairns serves as a consultant to bioMerieux and is funded for a grant from Bill & Melinda Gates Foundation. James A Overton is a consultant at Knocean Inc. Jessica Lasky-Su serves as a scientific advisor of Precion Inc. Scott R. Hutton, Greg Michelloti and Kari Wong are employees of Metabolon Inc. Vicki Seyfer- Margolis is a current employee of MyOwnMed. Nadine Rouphael reports contracts with Lilly and Sanofi for COVID-19 clinical trials and serves as a consultant for ICON EMMES for consulting on safety for COVID19 clinical trials. Adeeb Rahman is a current employee of Immunai Inc. Steven Kleinstein is a consultant related to ImmPort data repository for Peraton. Nathan Grabaugh is a consultant for Tempus Labs and the National Basketball Association. Akiko Iwasaki is a consultant for 4BIO, Blue Willow Biologics, Revelar Biotherapeutics, RIGImmune, Xanadu Bio, Paratus Sciences. Monica Kraft receives research funds paid to her institution from NIH, ALA; Sanofi, Astra-Zeneca for work in asthma, serves as a consultant for Astra-Zeneca, Sanofi, Chiesi, GSK for severe asthma; is a co-founder and CMO for RaeSedo, Inc, a company created to develop peptidomimetics for treatment of inflammatory lung disease. Esther Melamed received research funding from Babson Diagnostics, honorarium from Multiple Sclerosis Association of America and has served on advisory boards of Genentech, Horizon, Teva and Viela Bio. Carolyn Calfee receives research funding from NIH, FDA, DOD, Roche-Genentech and Quantum Leap Healthcare Collaborative as well as consulting services for Janssen, Vasomune, Gen1e Life Sciences, NGMBio, and Cellenkos. Wade Schulz was an investigator for a research agreement, through Yale University, from the Shenzhen Center for Health Information for work to advance intelligent disease prevention and health promotion; collaborates with the National Center for Cardiovascular Diseases in Beijing; is a technical consultant to Hugo Health, a personal health information platform; cofounder of Refactor Health, an AI-augmented data management platform for health care; and has received grants from Merck and Regeneron Pharmaceutical for research related to COVID-19.

Conflict of interest: The Icahn School of Medicine at Mount Sinai has filed patent applications related to SARS-CoV-2 serological assays and NDV-based SARS-CoV-2 vaccines, which list FK as co-inventor (Tech ID 200314G/US 17/913,783; Tech ID 200502G/US 17/922,777; Tech ID 211012G/PCT/US2022/077254; Tech ID 220404G/PCT/US2023/065225). Mount Sinai has created a company, Kantaro, to market serological tests for SARS-CoV-2. FK has consulted for Merck and Pfizer (before 2020) and is currently consulting for Pfizer, Seqirus, 3rd Rock Ventures, Merck, and Avimex. FK's laboratory is also collaborating with Pfizer on animal models of SARS-CoV-2. OL is a named inventor on patents held by Boston Children's Hospital relating to vaccine adjuvants and human in vitro platforms that model vaccine action (IDs US20150152385A1, WO2019099578A1). He is a cofounder of Ovax, Inc; has consulted for GlaxoSmithKline (GSK) and Hillevax; and leads a laboratory that has received research support from GSK. CBC serves as a consultant to bioMérieux. NR reports contracts with Lilly and Sanofi for COVID-19 clinical trials and serves as a consultant for ICON EMMES regarding safety for COVID-19 clinical trials. SHK is a consultant for ImmPort data repository for Peraton. MK receives funding from Sanofi and AstraZeneca for work in asthma and serves as a consultant for Sanofi, Chiesi, and GSK for severe asthma. EM received research funding from Babson Diagnostics and has served on the advisory boards of Genentech, Horizon, Teva, and Viela Bio.

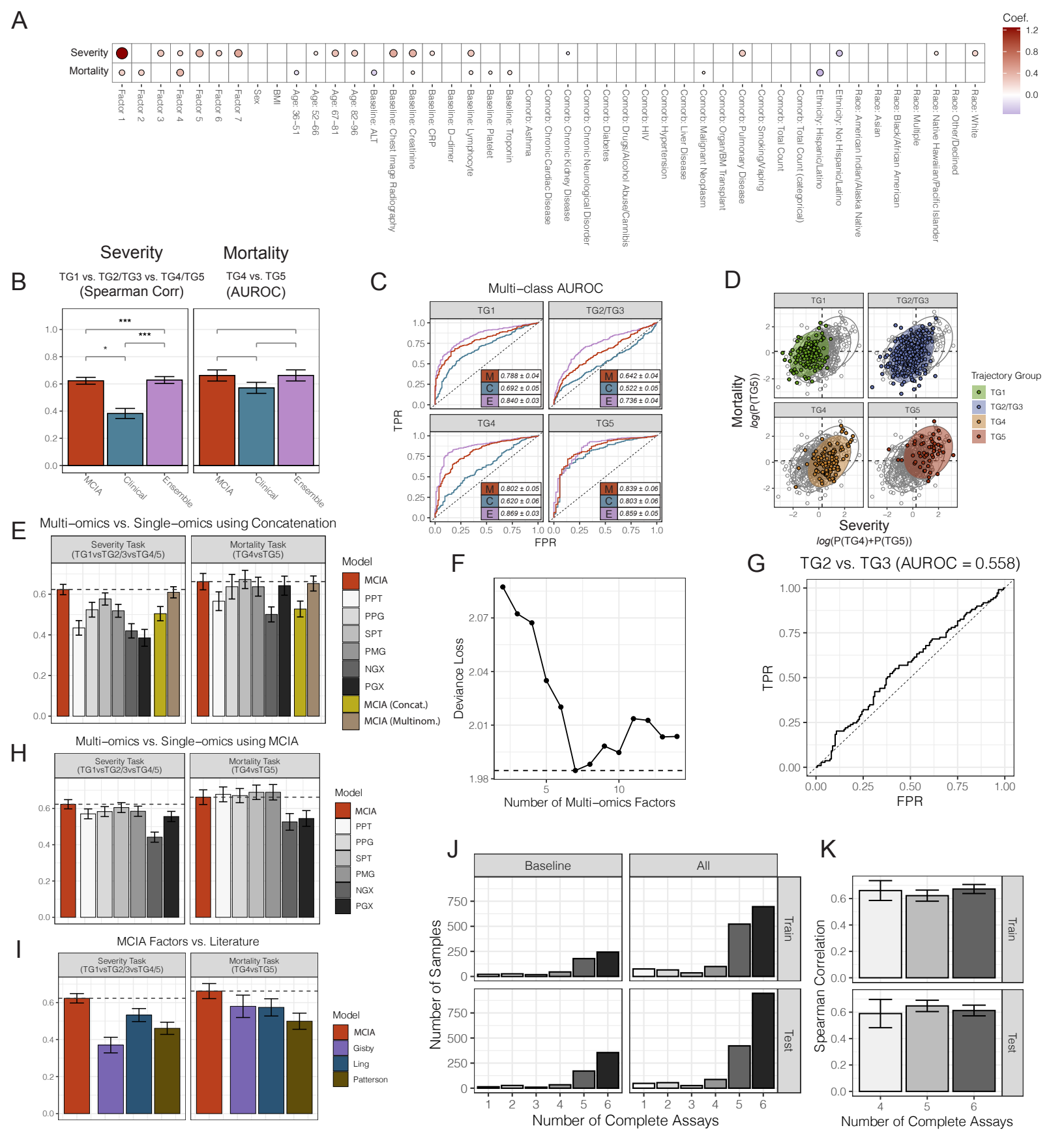
A
Coef.
1.2
0.8
0.4
0.0
Severity
Mortality
Factor 1
Factor 2
Factor 3
Factor 4
Factor 5
Factor 6
Factor 7
Sex
BMI
Age: 36–51
Age: 52–66
Age: 67–81
Age: 82–96
Baseline: ALT
Baseline: Chest Image Radiography
Baseline: Creatinine
Baseline: CRP
Baseline: D–dimer
Baseline: Lymphocyte
Baseline: Platelet
Baseline: Troponin
Comorb: Asthma
Comorb: Chronic Cardiac Disease
Comorb: Chronic Kidney Disease
Comorb: Chronic Neurological Disorder
Comorb: Diabetes
Comorb: Drugs/Alcohol Abuse/Cannibis
Comorb: HIV
Comorb: Hypertension
Comorb: Liver Disease
Comorb: Malignant Neoplasm
Comorb: Organ/BM Transplant
Comorb: Pulmonary Disease
Comorb: Smoking/Vaping
Comorb: Total Count
Comorb: Total Count (categorical)
Ethnicity: Hispanic/Latino
Ethnicity: Not Hispanic/Latino
Race: American Indian/Alaska Native
Race: Asian
Race: Black/African American
Race: Multiple
Race: Native Hawaiian/Pacific Islander
Race: Other/Declined
Race: White
B
Severity
Mortality
TG1 vs. TG2/TG3 vs. TG4/TG5
(Spearman Corr)
TG4 vs. TG5
(AUROC)
***
***
*
MCIA
Clinical
Ensemble
C
Multi–class AUROC
TG1
TG2/TG3
TG4
TG5
M 0.788 ± 0.04
C 0.692 ± 0.05
E 0.840 ± 0.03
M 0.642 ± 0.04
C 0.522 ± 0.05
E 0.736 ± 0.04
M 0.802 ± 0.05
C 0.620 ± 0.06
E 0.869 ± 0.03
M 0.839 ± 0.06
C 0.803 ± 0.06
E 0.859 ± 0.05
TPR
FPR
D
Mortality
log(P(TG5))
Severity
log(P(TG4)+P(TG5))
Trajectory Group
TG1
TG2/TG3
TG4
TG5
E
Multi–omics vs. Single–omics using Concatenation
Severity Task
(TG1vsTG2/3vsTG4/5)
Mortality Task
(TG4vsTG5)
Model
MCIA
PPT
PPG
SPT
PMG
NGX
PGX
MCIA (Concat.)
MCIA (Multinom.)
F
Deviance Loss
Number of Multi–omics Factors
G
TG2 vs. TG3 (AUROC = 0.558)
TPR
FPR
H
Multi–omics vs. Single–omics using MCIA
Severity Task
(TG1vsTG2/3vsTG4/5)
Mortality Task
(TG4vsTG5)
Model
MCIA
PPT
PPG
SPT
PMG
NGX
PGX
I
MCIA Factors vs. Literature
Severity Task
(TG1vsTG2/3vsTG4/5)
Mortality Task
(TG4vsTG5)
Model
MCIA
Gisby
Ling
Patterson
J
Baseline
All
Train
Test
Number of Samples
Number of Complete Assays
K
Train
Test
Spearman Correlation
Number of Complete Assays

FIGURE S1: Additional computational results for prediction models, severity and mortality task, and MOFA imputation, related to Figure 2. A) Dotplot of coefficients returned from the composite classifier, separated by MCIA factors and clinical features. B) Barplots of the severity and mortality tasks reporting Spearman correlation and AUROC values, respectively, on the training cohort. Results are shown for the MCIA, clinical, and ensemble models. C) Multi-class AUROC analysis predicting TG1, TG2/TG3, TG4, and TG5 separately for each model on the test cohort. D) Embedding of MCIA model predicted probabilities for both the mortality and severity tasks on the test cohort, faceted by each participant's TG. E) Severity and mortality task results on the training cohort for concatenated models. F) Connected scatter plot showing deviance loss of prediction models constructed using increasing numbers of multi-omics factors from MCIA. G) AUROC plot of MCIA model separating TG2 from TG3 on the training cohort. H, I) Severity and mortality task results on the training cohort for single-omic MCIA models and literature models. J) Histogram of participants grouped by the number of complete assays from PPT, PPG, SPT, PMG, NGX, and PGX, split by training/test (y-axis) and baseline/all visits (x-axis). K) Severity task results using only participants with 4, 5, and 6 complete assays on the training cohort.

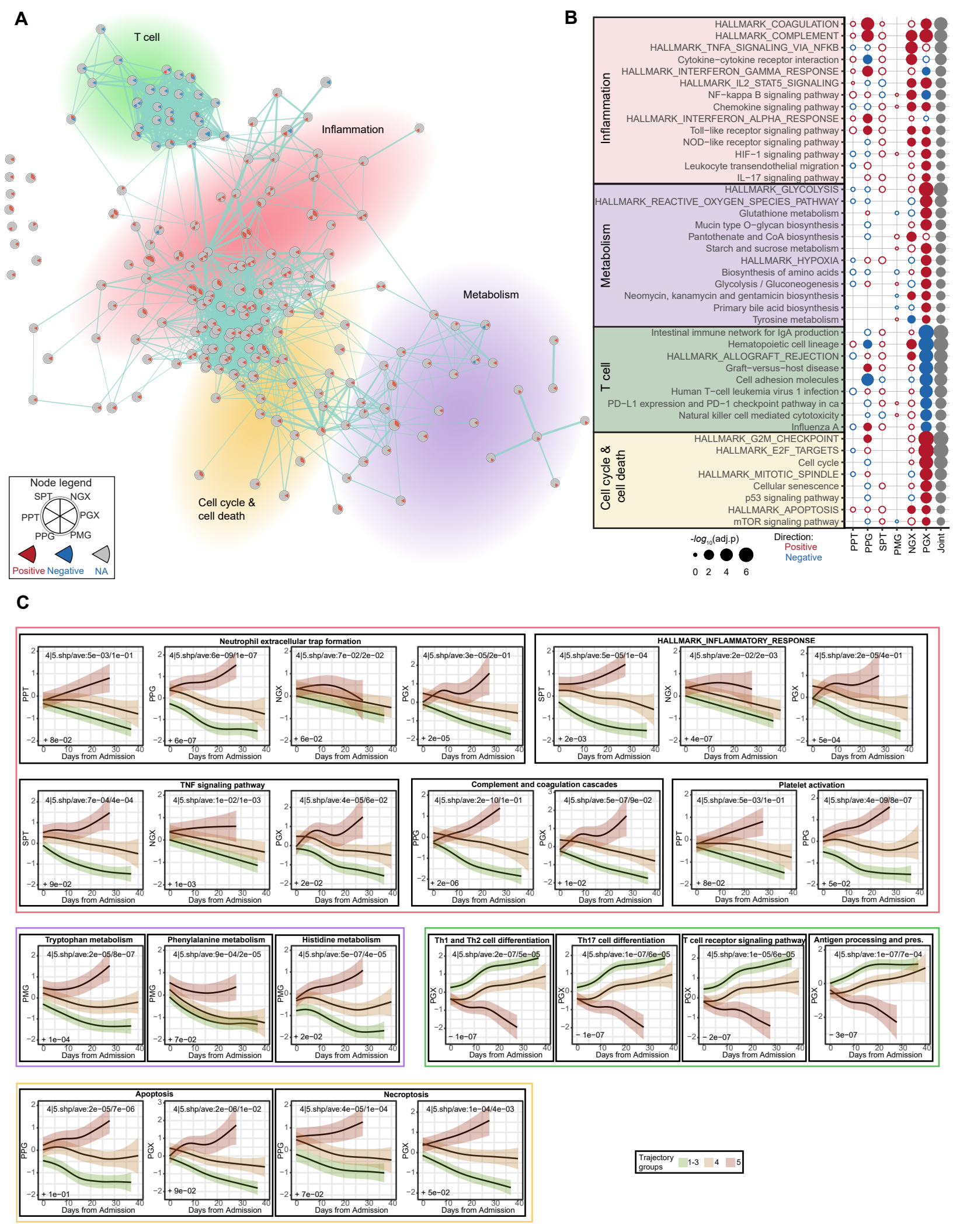
A
T cell
Inflammation
Metabolism
Cell cycle &
cell death
Node legend
SPT
NGX
PPT
PGX
PPG
PMG
Positive
Negative
NA
B
Inflammation
HALLMARK_COAGULATION
HALLMARK_COMPLEMENT
HALLMARK_TNFA_SIGNALING_VIA_NFKB
Cytokine−cytokine receptor interaction
HALLMARK_INTERFERON_GAMMA_RESPONSE
HALLMARK_IL2_STAT5_SIGNALING
NF−kappa B signaling pathway
Chemokine signaling pathway
HALLMARK_INTERFERON_ALPHA_RESPONSE
Toll−like receptor signaling pathway
NOD−like receptor signaling pathway
HIF−1 signaling pathway
Leukocyte transendothelial migration
IL−17 signaling pathway
Metabolism
HALLMARK_GLYCOLYSIS
HALLMARK_REACTIVE_OXYGEN_SPECIES_PATHWAY
Glutathione metabolism
Mucin type O−glycan biosynthesis
Pantothenate and CoA biosynthesis
Starch and sucrose metabolism
HALLMARK_HYPOXIA
Biosynthesis of amino acids
Glycolysis / Gluconeogenesis
Neomycin, kanamycin and gentamicin biosynthesis
Primary bile acid biosynthesis
Tyrosine metabolism
T cell
Intestinal immune network for IgA production
Hematopoietic cell lineage
HALLMARK_ALLOGRAFT_REJECTION
Graft−versus−host disease
Cell adhesion molecules
Human T−cell leukemia virus 1 infection
PD−L1 expression and PD−1 checkpoint pathway in ca
Natural killer cell mediated cytotoxicity
Influenza A
Cell cycle & cell death
HALLMARK_G2M_CHECKPOINT
HALLMARK_E2F_TARGETS
Cell cycle
HALLMARK_MITOTIC_SPINDLE
Cellular senescence
p53 signaling pathway
HALLMARK_APOPTOSIS
mTOR signaling pathway
PPT
PPG
SPT
PMG
NGX
PGX
Joint
-log10(adj.p)
0 2 4 6
Direction:
Positive
Negative
C
Neutrophil extracellular trap formation
HALLMARK_INFLAMMATORY_RESPONSE
TNF signaling pathway
Complement and coagulation cascades
Platelet activation
Tryptophan metabolism
Phenylalanine metabolism
Histidine metabolism
Th1 and Th2 cell differentiation
Th17 cell differentiation
T cell receptor signaling pathway
Antigen processing and pres.
Apoptosis
Necroptosis
Days from Admission
Trajectory groups
1-3
4
5

FIGURE S2: Enrichment term clustering and selected pathway trajectories for the severity factor, related to Figure 3. A) Visualization of functional enrichment using EnrichmentMap. The enriched terms are grouped based on biological functions as indicated using four colors and labels. The nodes correspond to enriched terms and each node is divided into six slices; each corresponds to one assay. The slices are colored based on the direction of enrichment: red if positive, blue if negative, and gray if the term is not tested or significantly enriched. The edge thickness corresponds to the number of shared leading-edge features between the terms. B) Pathway enrichment of severity factor for additional top enriched terms in each group in A apart from the ones in Fig 3C. The filled circles represent pathways with significant enrichment and the open circles without. Joint = aggregated p-value across omics. C) Trajectories for significant pathways in Fig 3C for different clinical trajectory groups. The p-values indicating whether the shape (shp) or average (avg) are significantly different between TG4 and TG5 are mentioned. TG1-TG3 are grouped together for better visualization.

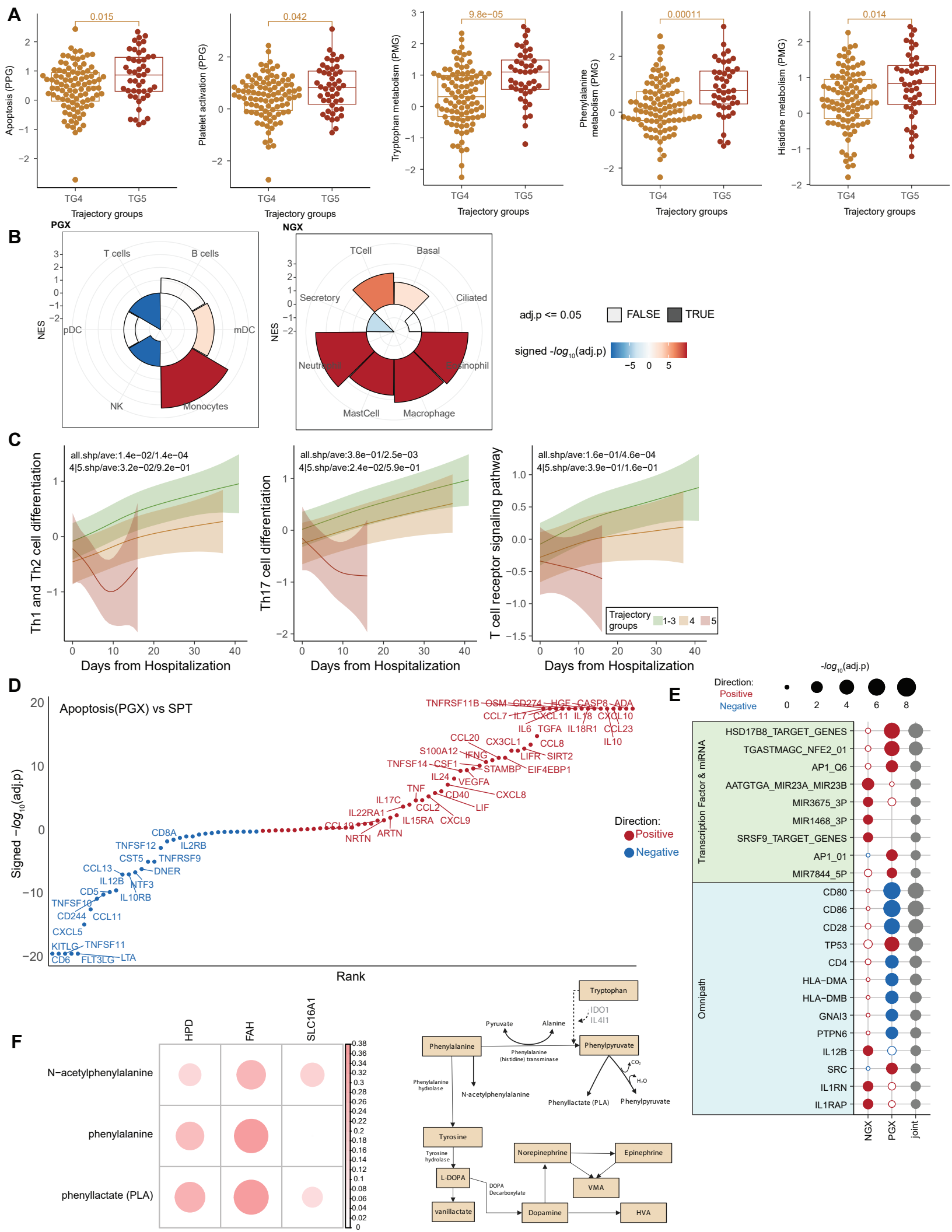
A
0.015
0.042
9.8e−05
0.00011
0.014
Apoptosis (PPG)
Platelet activation (PPG)
Tryptophan metabolism (PMG)
Phenylalanine metabolism (PMG)
Histidine metabolism (PMG)
TG4
TG5
Trajectory groups
B
PGX
NGX
T cells
B cells
pDC
mDC
NK
Monocytes
TCell
Basal
Secretory
Ciliated
Neutrophil
Eosinophil
MastCell
Macrophage
NES
adj.p <= 0.05
FALSE
TRUE
signed -log10(adj.p)
−5 0 5
C
all.shp/ave:1.4e−02/1.4e−04
4|5.shp/ave:3.2e−02/9.2e−01
all.shp/ave:3.8e−01/2.5e−03
4|5.shp/ave:2.4e−02/5.9e−01
all.shp/ave:1.6e−01/4.6e−04
4|5.shp/ave:3.9e−01/1.6e−01
Th1 and Th2 cell differentiation
Th17 cell differentiation
T cell receptor signaling pathway
Days from Hospitalization
Trajectory groups
1-3
4
5
D
Apoptosis(PGX) vs SPT
Signed −log10(adj.p)
Rank
TNFRSF11B
OSM
CD274
HGF
CASP8
ADA
CCL7
IL7
CXCL11
IL18
CXCL10
IL6
TGFA
IL18R1
CCL23
IL10
CCL20
CX3CL1
CCL8
S100A12
IFNG
LIFR
SIRT2
TNFSF14
CSF1
STAMBP
EIF4EBP1
IL24
VEGFA
TNF
CD40
CXCL8
IL17C
CCL2
LIF
IL22RA1
IL15RA
CXCL9
CCL19
NRTN
ARTN
CD8A
IL2RB
TNFSF12
TNFRSF9
CST5
DNER
CCL13
IL12B
NTF3
CD5
IL10RB
TNFSF10
CD244
CCL11
CXCL5
KITLG
TNFSF11
CD6
FLT3LG
LTA
Direction:
Positive
Negative
E
-log10(adj.p)
Direction:
Positive
Negative
0 2 4 6 8
Transcription Factor & miRNA
HSD17B8_TARGET_GENES
TGASTMAGC_NFE2_01
AP1_Q6
AATGTGA_MIR23A_MIR23B
MIR3675_3P
MIR1468_3P
SRSF9_TARGET_GENES
AP1_01
MIR7844_5P
Omnipath
CD80
CD86
CD28
TP53
CD4
HLA−DMA
HLA−DMB
GNAI3
PTPN6
IL12B
SRC
IL1RN
IL1RAP
NGX
PGX
joint
F
HPD
FAH
SLC16A1
N−acetylphenylalanine
phenylalanine
phenyllactate (PLA)
0.38
0.36
0.34
0.32
0.3
0.28
0.26
0.24
0.22
0.2
0.18
0.16
0.14
0.12
0.1
0.08
0.06
0.04
0.02
0
Tryptophan
IDO1
IL4I1
Pyruvate
Alanine
Phenylalanine
Phenylalanine (histidine) transminase
Phenylpyruvate
CO2
H2O
Phenylalanine hydrolase
N-acetylphenylalanine
Phenyllactate (PLA)
Phenylpyruvate
Tyrosine
Tyrosine hydrolase
Norepinephrine
Epinephrine
L-DOPA
DOPA Decarboxylate
VMA
vanillactate
Dopamine
HVA

FIGURE S3: Additional characterization of immune pathway associated with COVID-19 severity, related to Figures 3 and 4. For the **severity factor**, A) Boxplots comparing levels of identified pathways (from Fig 3F) with moderate separating power between TG4 and TG5 at baseline (p.val < 0.05). B) Cell type enrichment of the PBMC (PGX) and nasal (NGX) transcriptomics based on their contribution to the severity factor. C) Trajectory plots depicting differences in PBMC transcriptomic signature of T cell pathways (sum of levels of all pathway features corrected for T cell frequencies) between trajectory groups. The Th1 and Th2 cell differentiation and Th17 cell differentiation pathways show significant decrease in TG5 compared to TG4 (4|5). T cell receptor signaling pathway is not significant, but the trend is preserved. D) Correlation between high-contribution cytokines and the apoptosis pathway activity constructed using PBMC transcriptomics (PGX). The cytokines are ranked based on the adj.p on X-axis and the cytokines with significant associations (adj.p < 0.05) are labeled. E) mHG Enrichment of the target genes of Transcription Factors and miRNAs (C3), and the downstream targets of receptor signaling (Omnipath) in the highly contributing PGX and NGX features of the severity factor. The filled circles represent pathways with significant enrichment and the open circles without. Joint = aggregated p-value across omics. F) The left panel displays the correlation between metabolites in the phenylalanine pathway and genes identified to play a role in actively converting phenylpyruvate from phenylalanine. The right panel features a simplified diagram of the tryptophan, phenylalanine, and tyrosine pathways. IDO1 can also degrade phenylalanine to phenylpyruvate, which can lead to a decrease in phenylalanine hydroxylase activity and an accumulation of phenylalanine in the body. The tyrosine metabolites (HVA, VMA, and VLA) are major terminal urinary metabolites that result from the conversion of L-Dopa, dopamine, and norepinephrine during catecholamine biosynthesis and degradation.

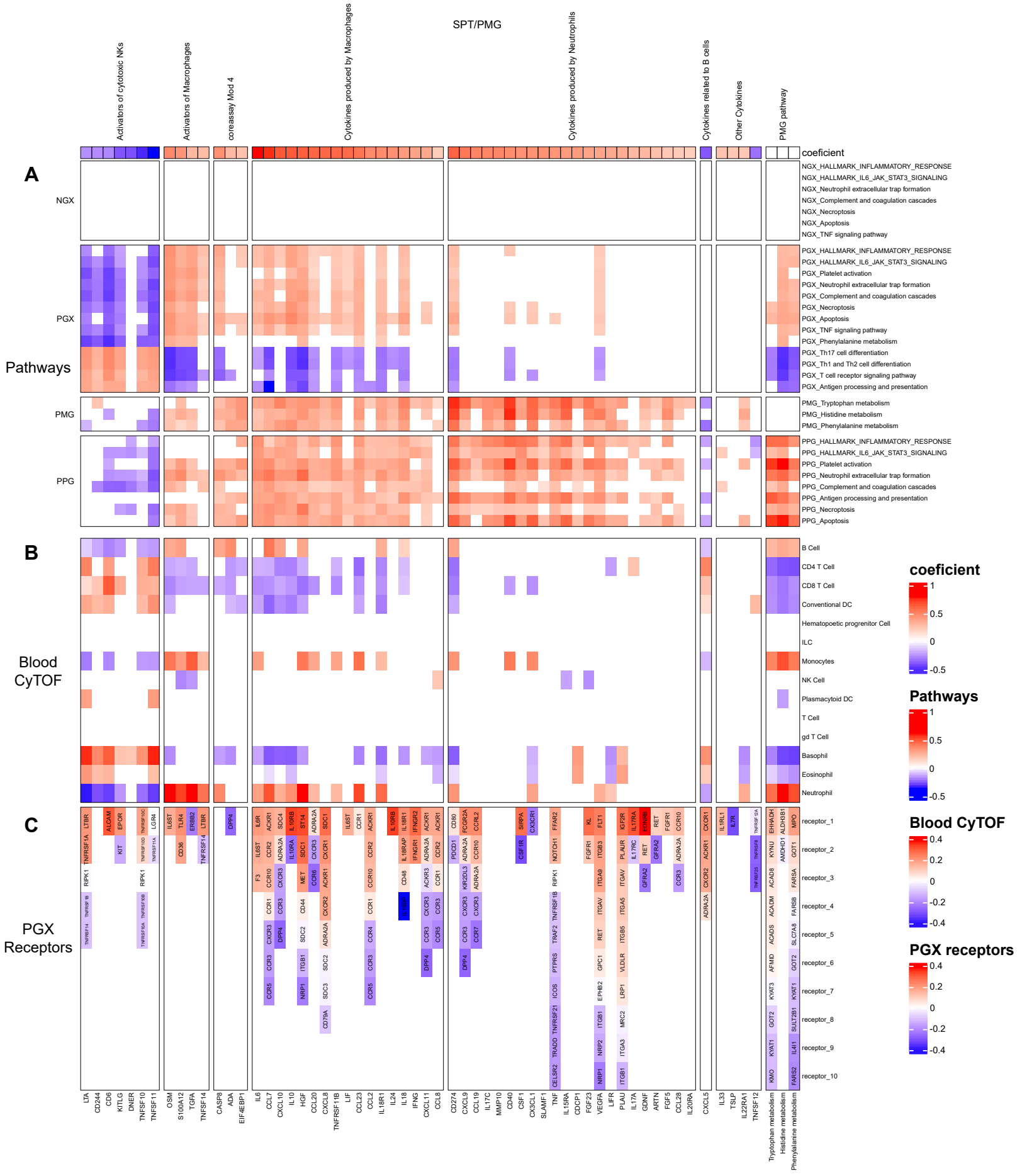
SPT/PMG
Activators of cytotoxic NKs
Activators of Macrophages
coreassay Mod 4
Cytokines produced by Macrophages
Cytokines produced by Neutrophils
Cytokines related to B cells
Other Cytokines
PMG pathway
coeficient
A
NGX
PGX
Pathways
PMG
PPG
NGX_HALLMARK_INFLAMMATORY_RESPONSE
NGX_HALLMARK_IL6_JAK_STAT3_SIGNALING
NGX_Neutrophil extracellular trap formation
NGX_Complement and coagulation cascades
NGX_Necroptosis
NGX_Apoptosis
NGX_TNF signaling pathway
PGX_HALLMARK_INFLAMMATORY_RESPONSE
PGX_HALLMARK_IL6_JAK_STAT3_SIGNALING
PGX_Platelet activation
PGX_Neutrophil extracellular trap formation
PGX_Complement and coagulation cascades
PGX_Necroptosis
PGX_Apoptosis
PGX_TNF signaling pathway
PGX_Phenylalanine metabolism
PGX_Th17 cell differentiation
PGX_Th1 and Th2 cell differentiation
PGX_T cell receptor signaling pathway
PGX_Antigen processing and presentation
PMG_Tryptophan metabolism
PMG_Histidine metabolism
PMG_Phenylalanine metabolism
PPG_HALLMARK_INFLAMMATORY_RESPONSE
PPG_HALLMARK_IL6_JAK_STAT3_SIGNALING
PPG_Platelet activation
PPG_Neutrophil extracellular trap formation
PPG_Complement and coagulation cascades
PPG_Antigen processing and presentation
PPG_Necroptosis
PPG_Apoptosis
B
Blood CyTOF
B Cell
CD4 T Cell
CD8 T Cell
Conventional DC
Hematopoetic progrenitor Cell
ILC
Monocytes
NK Cell
Plasmacytoid DC
T Cell
gd T Cell
Basophil
Eosinophil
Neutrophil
C
PGX Receptors
receptor_1
receptor_2
receptor_3
receptor_4
receptor_5
receptor_6
receptor_7
receptor_8
receptor_9
receptor_10
LTA
CD244
CD6
KITLG
DNER
TNFSF10
TNFSF11
OSM
S100A12
TGFA
TNFSF14
CASP8
ADA
EIF4EBP1
IL6
CCL7
CXCL10
IL10
HGF
CCL20
CXCL8
TNFRSF11B
LIF
CCL23
CCL2
IL18R1
IL24
IL18
IFNG
CXCL11
CCL8
CD274
CXCL9
CCL19
IL17C
MMP10
CD40
CSF1
CX3CL1
SLAMF1
TNF
IL15RA
CDCP1
FGF23
VEGFA
LIFR
PLAU
IL17A
GDNF
ARTN
FGF5
CCL28
IL20RA
CXCL5
IL33
TSLP
IL22RA1
TNFSF12
Tryptophan metabolism
Histidine metabolism
Phenylalanine metabolism
coeficient
1
0.5
0
-0.5
Pathways
1
0.5
0
-0.5
Blood CyTOF
0.4
0.2
0
-0.2
-0.4
PGX receptors
0.4
0.2
0
-0.2
-0.4

FIGURE S4: Inter-omics analysis on top-contribution cytokines and significant pathways for the severity factor, related to Figures 3 and 4. Serum soluble proteins were grouped into six WGCNA clusters previously defined in *Diray-Arce, et al.*[23], alongside the top three pathways identified in PMG. All correlation matrices were generated by controlling covariates such as sex, admission date, and enrollment site. A) Correlation of Serum soluble proteins and Tryptophan, Histidine, and Phenylalanine metabolism with the top pathways from PMG, PPG, NGX, and PGX in the severity Factor. NGX data did not show significant trans-omics correlations. Cytokines produced by neutrophils positively correlate with PMG and PPG pathways. Similarly, cytokines produced by macrophages and activators of Macrophages positively correlate with all other omics pathways. Additionally, we found a negative association between activators of cytotoxic NKs, which are negatively associated with severity factors, and other omics pathways. B) Correlation of parent cell type population, serum soluble proteins and Tryptophan, Histidine, and Phenylalanine metabolism. Monocytes and neutrophils showed positive correlation with PMG pathways. C) The reported receptors in CellTalkDb for the serum soluble proteins and their strength in the severity Factor. We showed the top 10 receptors per serum soluble proteins and metabolite pathway.

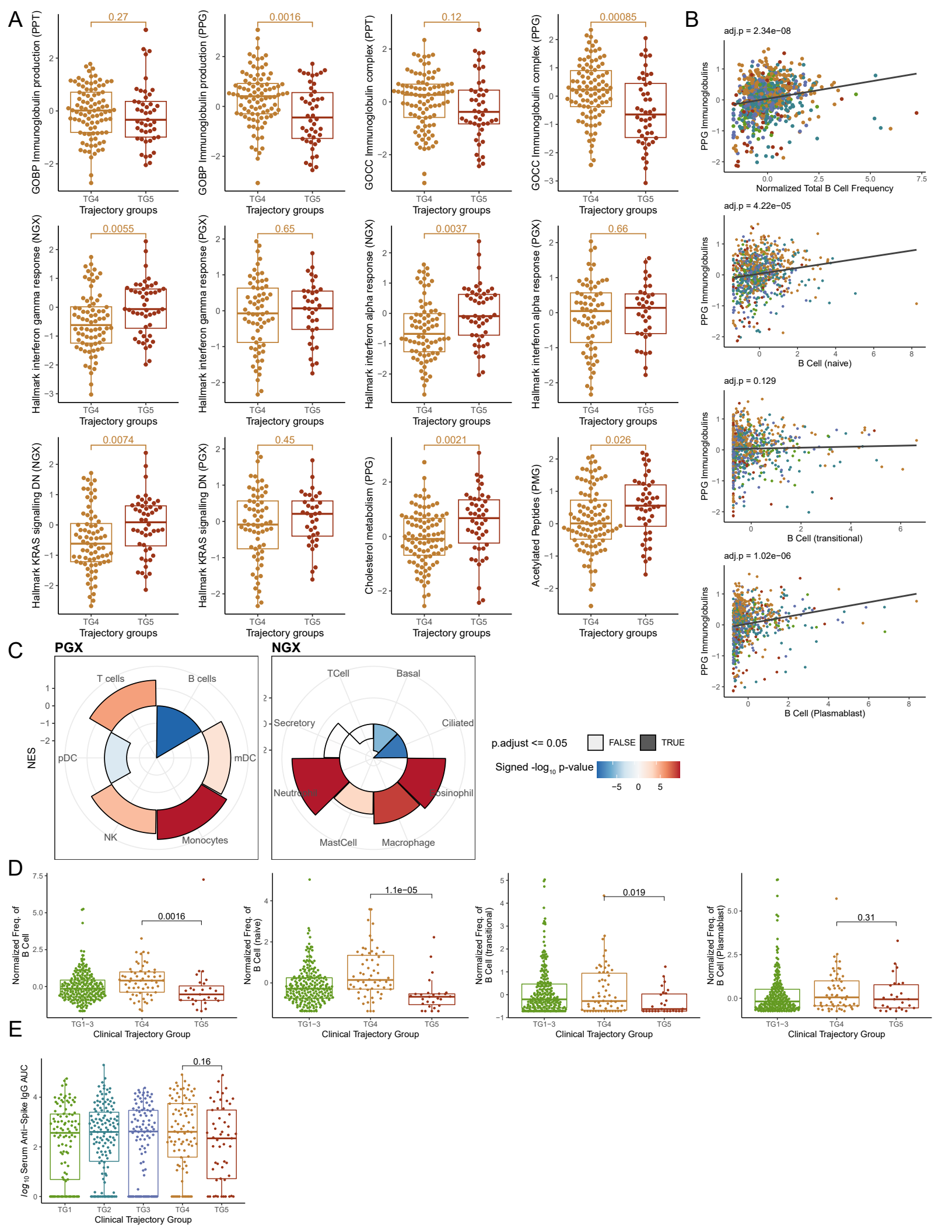
A
GOBP Immunoglobulin production (PPT)
0.27
GOBP Immunoglobulin production (PPG)
0.0016
GOCC Immunoglobulin complex (PPT)
0.12
GOCC Immunoglobulin complex (PPG)
0.00085
Hallmark interferon gamma response (NGX)
0.0055
Hallmark interferon gamma response (PGX)
0.65
Hallmark interferon alpha response (NGX)
0.0037
Hallmark interferon alpha response (PGX)
0.66
Hallmark KRAS signalling DN (NGX)
0.0074
Hallmark KRAS signalling DN (PGX)
0.45
Cholesterol metabolism (PPG)
0.0021
Acetylated Peptides (PMG)
0.026
TG4
TG5
Trajectory groups
B
adj.p = 2.34e−08
adj.p = 4.22e−05
adj.p = 0.129
adj.p = 1.02e−06
PPG Immunoglobulins
Normalized Total B Cell Frequency
B Cell (naive)
B Cell (transitional)
B Cell (Plasmablast)
C
PGX
NGX
NES
T cells
B cells
pDC
mDC
NK
Monocytes
TCell
Basal
Secretory
Ciliated
Neutrophil
Eosinophil
MastCell
Macrophage
p.adjust <= 0.05
FALSE
TRUE
Signed -log10 p-value
−5
0
5
D
Normalized Freq. of B Cell
0.0016
Normalized Freq. of B Cell (naive)
1.1e−05
Normalized Freq. of B Cell (transitional)
0.019
Normalized Freq. of B Cell (Plasmablast)
0.31
TG1−3
TG4
TG5
Clinical Trajectory Group
E
log10 Serum Anti−Spike IgG AUC
0.16
TG1
TG2
TG3
TG4
TG5
Clinical Trajectory Group

FIGURE S5: Additional characterization of immune pathway associated with COVID-19 mortality, related to Figure 5. For the **mortality factor,** A) Boxplots comparing TG4 and TG5 at baseline across assays for enriched mortality factor pathway (adj.pval < 0.1) that separated by at least one measured omics (p.val < 0.05). B) Scatter plot between PPG (plasma proteomics global) immunoglobulin levels and total B cells/B cell subpopulation normalized frequencies. Significance was calculated using a linear mixed effect model (see Supplemental Methods, Inter-omics association analysis). C) Cell type enrichment of the PBMC and nasal transcriptomics based on their contribution to the mortality factor. D) Boxplots of total B cell normalized frequency and top associated B-cell subpopulations across TG groups at baseline. E) Boxplot of log10 Serum Anti-Spike IgG titers across TG groups at baseline.

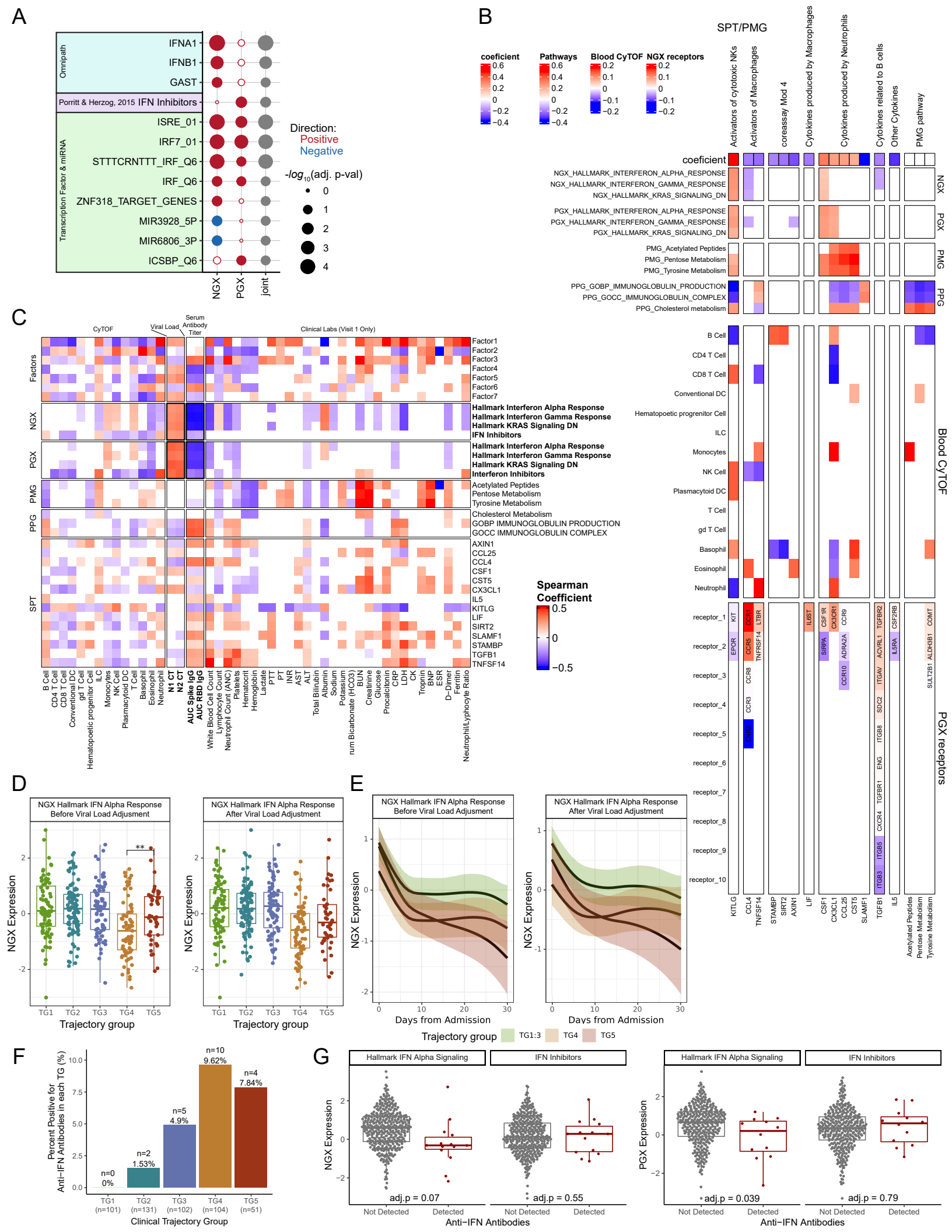
A
Omnipath
IFNA1
IFNB1
GAST
Porritt & Herzog, 2015 IFN Inhibitors
Transcription Factor & miRNA
ISRE_01
IRF7_01
STTTCRNTTT_IRF_Q6
IRF_Q6
ZNF318_TARGET_GENES
MIR3928_5P
MIR6806_3P
ICSBP_Q6
NGX
PGX
joint
Direction:
Positive
Negative
-log10(adj. p-val)
0
1
2
3
4
B
SPT/PMG
coeficient
Pathways
Blood CyTOF
NGX receptors
Activators of cytotoxic NKs
Activators of Macrophages
coreassay Mod 4
Cytokines produced by Macrophages
Cytokines produced by Neutrophils
Cytokines related to B cells
Other Cytokines
PMG pathway
NGX_HALLMARK_INTERFERON_ALPHA_RESPONSE
NGX_HALLMARK_INTERFERON_GAMMA_RESPONSE
NGX_HALLMARK_KRAS_SIGNALING_DN
PGX_HALLMARK_INTERFERON_ALPHA_RESPONSE
PGX_HALLMARK_INTERFERON_GAMMA_RESPONSE
PGX_HALLMARK_KRAS_SIGNALING_DN
PMG_Acetylated Peptides
PMG_Pentose Metabolism
PMG_Tyrosine Metabolism
PPG_GOBP_IMMUNOGLOBULIN_PRODUCTION
PPG_GOCC_IMMUNOGLOBULIN_COMPLEX
PPG_Cholesterol metabolism
C
CyTOF
Viral Load
Serum Antibody Titer
Clinical Labs (Visit 1 Only)
Factors
NGX
PGX
PMG
PPG
SPT
Factor1
Factor2
Factor3
Factor4
Factor5
Factor6
Factor7
Hallmark Interferon Alpha Response
Hallmark Interferon Gamma Response
Hallmark KRAS Signaling DN
IFN Inhibitors
Hallmark Interferon Alpha Response
Hallmark Interferon Gamma Response
Hallmark KRAS Signaling DN
Interferon Inhibitors
Acetylated Peptides
Pentose Metabolism
Tyrosine Metabolism
Cholesterol Metabolism
GOBP IMMUNOGLOBULIN PRODUCTION
GOCC IMMUNOGLOBULIN COMPLEX
AXIN1
CCL25
CCL4
CSF1
CST5
CX3CL1
IL5
KITLG
LIF
SIRT2
SLAMF1
STAMBP
TGFB1
TNFSF14
Spearman Coefficient
0.5
0
−0.5
B Cell
CD4 T Cell
CD8 T Cell
Conventional DC
Hematopoetic progenitor Cell
ILC
Monocytes
NK Cell
Plasmacytoid DC
T Cell
gd T Cell
Basophil
Eosinophil
Neutrophil
N1 CT
N2 CT
AUC Spike IgG
AUC RBD IgG
White Blood Cell Count
Lymphocyte Count
Neutrophil Count (ANC)
Platelets
Hematocrit
Hemoglobin
Lactate
PTT
PT
INR
AST
ALT
Total Bilirubin
Albumin
Sodium
Potassium
Bicarbonate (HCO3)
BUN
Creatinine
Glucose
Procalcitonin
CRP
LDH
CK
Troponin
BNP
ESR
D−Dimer
Ferritin
Neutrophil/Lymphocyte Ratio
Blood CyTOF
PGX receptors
receptor_1
receptor_2
receptor_3
receptor_4
receptor_5
receptor_6
receptor_7
receptor_8
receptor_9
receptor_10
KIT
EPOR
CCR1
CCR5
CCR8
CCR3
CXCR2
LTBR
TNFRSF14
IL6ST
CSF1R
SIRPA
CX3CR1
CCR9
CCR10
ADRA2A
ACVRL1
TGFBR2
ITGAV
SDC2
ITGB8
ENG
TGFBR1
CXCR4
ITGB5
ITGB3
IL5RA
CSF2RB
SULT2B1
ALDH3B1
COMT
KITLG
CCL4
TNFSF14
STAMBP
SIRT2
AXIN1
LIF
CSF1
CX3CL1
CCL25
CST5
SLAMF1
TGFB1
IL5
Acetylated Peptides
Pentose Metabolism
Tyrosine Metabolism
D
NGX Hallmark IFN Alpha Response
Before Viral Load Adjusment
After Viral Load Adjustment
NGX Expression
**
TG1
TG2
TG3
TG4
TG5
Trajectory group
E
NGX Hallmark IFN Alpha Response
Before Viral Load Adjusment
After Viral Load Adjustment
NGX Expression
Days from Admission
Trajectory group
TG1:3
TG4
TG5
F
Percent Positive for Anti−IFN Antibodies in each TG (%)
n=0
0%
n=2
1.53%
n=5
4.9%
n=10
9.62%
n=4
7.84%
TG1 (n=101)
TG2 (n=131)
TG3 (n=102)
TG4 (n=104)
TG5 (n=51)
Clinical Trajectory Group
G
Hallmark IFN Alpha Signaling
IFN Inhibitors
NGX Expression
PGX Expression
adj.p = 0.07
adj.p = 0.55
adj.p = 0.039
adj.p = 0.79
Not Detected
Detected
Anti−IFN Antibodies

FIGURE S6: Additional characterization of interferon signaling, anti-IFN auto-antibodies, and inter-omics analysis of top-contribution cytokines and significant pathways for the severity factor, related to Figures 5 and 6. A) mHG Enrichment of Transcription Factors and miRNA (C3), IFN inhibitors, and downstream receptor signaling (Omnipath) for PBMC and Nasal Transcriptomics associated with the Mortality Factor. Joint = aggregated p-value across omics. B) Top: Spearman Correlation of top metabolic pathways and SPT soluble proteins against significant mortality associated pathways in the PMG, PPG, NGX, and PGX. Middle: Spearman Correlation of top metabolic pathways and SPT soluble proteins against whole blood CyTOF parent population frequencies. Bottom: Spearman Correlation of top metabolic pathways and SPT soluble proteins against their receptors' expression in the PGX (CelltalkDB for SPT and RaMP for PMG). C) Spearman Correlation of Trans-omic Severity and Mortality associated biological pathways/features with additional omics including whole blood CyTOF cell type frequency, nasal viral load (inverted RT-qPCR CT), Anti-Spike and Anti-RPB Antibody Titers, and Baseline Clinical laboratory tests. Non-significant correlations are white. D) Nasal and PBMC Hallmark Interferon alpha response at visit 1 between clinical trajectory groups unadjusted and adjusted for nasal viral load. E) Nasal Hallmark Interferon alpha response over 30 days unadjusted and adjusted for nasal viral load. F) Presence of Anti-IFN antibodies per clinical trajectory group. G) Hallmark IFN alpha response and expression of IFN inhibitors in Nasal and PBMC transcriptomics at visit 1 for participants with and without detectable anti-IFN antibodies.

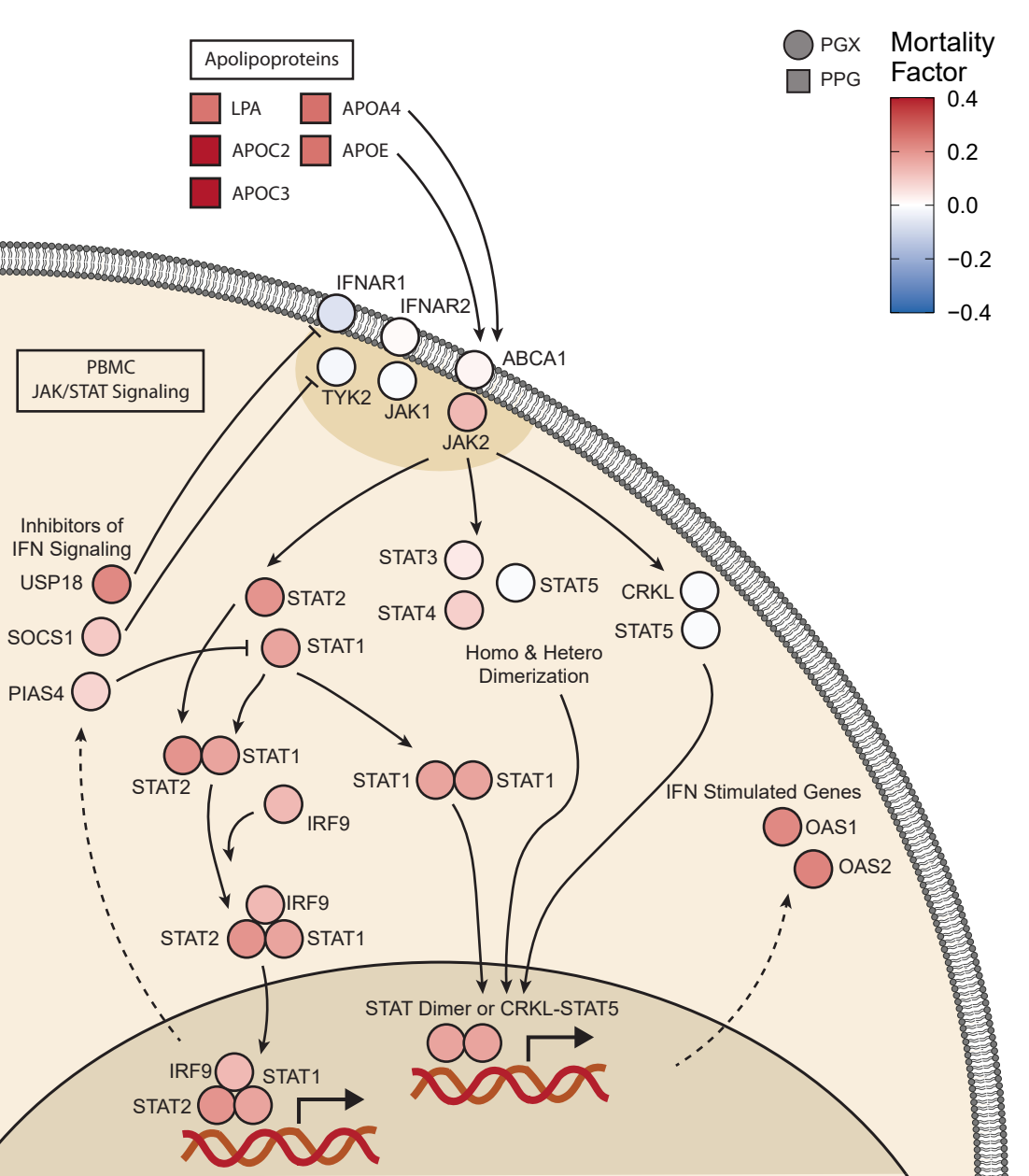
Apolipoproteins
LPA
APOA4
APOC2
APOE
APOC3
PGX
PPG
Mortality Factor
0.4
0.2
0.0
−0.2
−0.4
IFNAR1
IFNAR2
ABCA1
TYK2
JAK1
JAK2
PBMC JAK/STAT Signaling
Inhibitors of IFN Signaling
USP18
SOCS1
PIAS4
STAT2
STAT1
STAT3
STAT4
STAT5
CRKL
STAT5
Homo & Hetero Dimerization
STAT1
STAT2
IRF9
STAT1
STAT1
IFN Stimulated Genes
OAS1
OAS2
IRF9
STAT2
STAT1
STAT Dimer or CRKL-STAT5
IRF9
STAT1
STAT2

FIGURE S7: Virus-centered integrative multi-omics network of the mortality(-associated) factor (Factor 4) in PGX, related to Figure 6. IFN signaling is enriched in both the NGX (Fig 6) and PGX (Fig S7). Key IFN signaling is associated with the mortality factor in the PGX including STAT gene expression, ISGs, and downstream upregulation of IFN inhibitors which can generate negative feedback and inhibit upstream signaling.

Supplemental Table 11: Key resources

REAGENT or RESOURCE	SOURCE	IDENTIFIER
Antibodies		
Maxpar® Direct™ Immune Profiling Assay (MDIPA) Kit	Fluidigm	Cat#201325
CD8a-146Nd	Fluidigm	Cat#3146001B; RRID:AB_2687641
Granzyme B Antibody, anti-human/mouse/rat, REAfinity	Miltenyi	Cat#130-116-486
Goat Anti-Human IgA-UNLB	Southern Biotech	Cat#2050-01
Purified anti-human IgM Antibody	Biolegend	Cat#314502
Mouse Anti-Human IgG1 Fc-UNLB	Souther Biotech	Cat#9054-01
Purified anti-mouse/human CD11b Antibody	Biolegend	Cat#101202
Purified anti-human/mouse/rat CD278 (ICOS) Antibody	Biolegend	Cat#313502
Purified anti-human CD39 Antibody	Biolegend	Cat#328202
Purified anti-human CD169 (Sialoadhesin, Siglec-1) Antibody	Biolegend	Cat#346002
Purified anti-human CD64 (Maxpar® Ready) Antibody	Biolegend	Cat#305029
Purified anti-human CD71 Antibody	Biolegend	Cat#334102
Anti-Human CD279/PD-1 (EH12.2H7)-175Lu	Fluidigm	Cat#3175008B
Anti-Human CD61 (VI-PL2)-209Bi	Fluidigm	Cat#3209001B
Anti-Human CD3 (UCHT1)-141Pr antibody	Fluidigm	Cat#3141019B
Anti-Human HLA-DR (L243)-143Nd antibody	Fluidigm	Cat#3143013B
Anti-Human CD69 (FN50)-144Nd antibody	Fluidigm	Cat#3144018B
Anti-Human CD4 (RPA-T4)-145Nd antibody	Fluidigm	Cat#3145001B
Anti-Human CD8a (RPA-T8)-146Nd antibody	Fluidigm	Cat#3146001B
Anti-Human CD20 (2H7)-147Sm antibody	Fluidigm	Cat#3147001B
Anti-Human CD127 (A019D5)-149Sm antibody	Fluidigm	Cat#3149011B
Anti-Human MIP-1β (D21-1351)-150Nd antibody	Fluidigm	Cat#3150004B
Anti-Human CD123 (6H6)-151Eu antibody	Fluidigm	Cat#3151001B
Anti-Human TNFα (Mab11)-152Sm antibody	Fluidigm	Cat#3152002B
Anti-Human CD62L (DREG-56)-153Eu antibody	Fluidigm	Cat#3153004B
Anti-Human CD45 (HI30)-154Sm antibody	Fluidigm	Cat#3154001B
Anti-Human IL-6 (MQ2-13A5)-156Gd antibody	Fluidigm	Cat#3156011B
Anti-Human IFN-γ (B27)-158Gd antibody	Fluidigm	Cat#3158017B
Anti-Human CD11c (Bu15)-159Tb antibody	Fluidigm	Cat#3159001B
Anti-Human CD14 (M5E2)-160Gd antibody	Fluidigm	Cat#3160001B
Anti-Human CD80/B7.1 (2D10.4)-161Dy antibody	Fluidigm	Cat#3161023B
Anti-Human CD66b (80H3)-162Dy antibody	Fluidigm	Cat#3162023B
Anti-Human CD56 (NCAM16.2)-163Dy antibody	Fluidigm	Cat#3163007B
Anti-Human CD15 (W6D3)-164Dy antibody	Fluidigm	Cat#3164001B
Anti-Human CD61 (VI-PL2)-165Ho antibody	Fluidigm	Cat#3165010B
Anti-Human CD11b (ICRF44)-167Er antibody	Fluidigm	Cat#3167011B
Anti-Human CD206 (15-2)-168Er antibody	Fluidigm	Cat#3168008B
Anti-Human CD54 (HA58)-170Er antibody	Fluidigm	Cat#3170014B
Anti-Human CD68 (Y1/82A)-171Yb antibody	Fluidigm	Cat#3171011B
Anti-Human CD16 (3G8)-209Bi antibody	Fluidigm	Cat#3209002B
Anti- CoV Nucleocapsid protein (6H3) antibody	Abcam	Cat#ab273434
Anti-Human Eotaxin (43915) antibody	R&D	Cat#MAB3201
Anti-Human ACE-2 (535919) antibody	NOVUS	Cat#MAB9332-100

Anti-Human Cytokeratin (C-11) antibody	Biolegend	Cat#628602
Anti- CoV Spike protein (1A9) antibody	GeneTex	Cat#GTX632604
Anti-Human EPX (MM82.2.1) antibody	MAYO CLINIC	https://www.mayoclinic.org
Anti-Human IL-8 (E8N1) antibody	Biolegend	Cat#511402
Anti-Human IL-1β (H1b-27) antibody	Biolegend	Cat#511602
Anti-Human IFN-β (IFNb/A1) antibody	Biolegend	Cat#514002
Anti-Human Siglec-8 (837535) antibody	R&D	Cat#MAB7975
Anti-human IgG (Fc specific)-Peroxidase antibody produced in goat	Sigma-Aldrich	Cat#A0170; RRID: AB_257868
Goat anti-human IgM-HRP	SouthernBiotech	Cat#2020-05; RRID: AB_2795603
Anti-human IgA (α-chain specific)-Peroxidase antibody produced in goat	Sigma-Aldrich	Cat#A0295; RRID: AB_257876
Anti-Glial Fibrillary Associated Protein	Agilent	Cat#Z033429-2
Anti-human IgG (PE)	ThermoScientific	Cat#12-4998-8
Anti-human pSTAT1 (AF647)	BD	Cat#612597
Anti-human CD14 (FITC)	BD	Cat#555397
Bacterial and virus strains		
BLT5403, T7 Select Kit	Novagen	Cat#70550-3
T7 Bacteriophage, T7 Select Kit	Novagen	Cat#70550-3
Biological samples		
Plasma samples from IMPACC cohort	Multiple clinical sites	N/A
Whole blood from hospitalized COVID19 patients-collected in EDTA tubes	Multiple clinical sites	N/A
Veri-Cells™ Heavy Metal (Ta) PBMC	Biolegend	Cat#427203
Serum samples from IMPACC cohort	Multiple clinical sites	N/A
Stimulated Plasma from Healthy Controls	Stanford University	N/A
Plasma from Healthy Controls	Stanford University	N/A
Serum from Healthy Controls	Stanford University	N/A
Chemicals, peptides, and recombinant proteins		
DNA/RNA Shield Collection Tube w/ Swab - DX	Zymo Research	Cat#R1107-E
Quick-DNA/RNA MagBead	Zymo Research	Cat#R2131
Stranded Total RNA Prep, Ligation with Ribo-Zero Plus	Illumina	Cat#20040529
HS NGS Fragment Kit	Agilent	Cat#DNF-474-0500
K-562 Total RNA	Thermo Fisher	Cat#AM7832
qScript XLT 1-Step RT-qPCR ToughMix	Quantabio	Cat#95133-02K
2-propanolol (LC-MS)	MilliporeSigma	Cat#1027814000
Acetonitrile (LC-MS)	MilliporeSigma	Cat# 1000294000
Water, Baker Analyzed LC/MS Reagent Grade	J.T. Baker	Cat#9831-02
Ammonium Formate (LC-MS)	J.T. Baker	Cat#M530-08
Perfluoropentanoic acid	Sigma	Cat#396575
Ammonium Bicarbonate	Fisher	Cat#A643
Ammonium Hydroxide	Sigma	Cat#338818
Cell-ID™ 20-Plex Pd Barcoding Kit	Fluidigm	Cat#201060
Saponin	Sigma	Cat#47036
Human TruStain FcX™ (Fc Receptor Blocking Solution)	Biolegend	Cat#422302; RRID:AB_2818986
Heparin sodium salt	Sigma	Cat#H3393

SmartTube PROT1 stabilizer PROT1-250ML	SmartTube	Fisher Cat# 501351692
SmartTube ThawLyse - THAWLYSE1	SmartTube	Fisher Cat# 501351696
Paraformaldehyde (PFA), 16% w/v aqueous, methanol-free	Alfa Aesar	Fisher Cat# AA433689L
Fetal bovine serum, characterized, heat-inactivated	HyClone	Fisher Cat#SH30396.03
Dimethyl sulfoxide	Fisher	Cat#BP231-100
Maxpar MCP9 Antibody Labeling Kit, 111Cd	Fluidigm	Cat#201111A
Maxpar MCP9 Antibody Labeling Kit, 112Cd	Fluidigm	Cat#201112A
Maxpar MCP9 Antibody Labeling Kit, 114Cd	Fluidigm	Cat#201114A
Maxpar MCP9 Antibody Labeling Kit, 116Cd	Fluidigm	Cat#201116A
Maxpar® X8 Antibody Labeling Kit, 142Nd	Fluidigm	Cat#201142B
Maxpar® X8 Antibody Labeling Kit, 159Tb	Fluidigm	Cat#201159B
Maxpar® X8 Antibody Labeling Kit, 162Dy	Fluidigm	Cat#201162B
Maxpar® X8 Antibody Labeling Kit, 165Ho	Fluidigm	Cat#201165B
Maxpar® X8 Antibody Labeling Kit, 169Tm	Fluidigm	Cat#201169B
Maxpar® X8 Antibody Labeling Kit, 142Nd—4 Rxn	Fluidigm	Cat#201142A
Maxpar® X8 Antibody Labeling Kit, 148Nd—4 Rxn	Fluidigm	Cat#201148A
Maxpar® X8 Antibody Labeling Kit, 155Gd—4 Rxn	Fluidigm	Cat#201155A
Maxpar® X8 Antibody Labeling Kit, 166Er—4 Rxn	Fluidigm	Cat#201166A
Maxpar® X8 Antibody Labeling Kit, 169Tm—4 Rxn	Fluidigm	Cat#201169A
Maxpar® X8 Antibody Labeling Kit, 172Er—4 Rxn	Fluidigm	Cat#201172A
Maxpar® X8 Antibody Labeling Kit, 173Yb—4 Rxn	Fluidigm	Cat#201173A
Maxpar® X8 Antibody Labeling Kit, 174Yb—4 Rxn	Fluidigm	Cat#201174A
Maxpar® X8 Antibody Labeling Kit, 175Lu—4 Rxn	Fluidigm	Cat#201175A
Maxpar® X8 Antibody Labeling Kit, 176Yb—4 Rxn	Fluidigm	Cat#201176A
Cell-ID™ Cisplatin	Fluidigm	Cat#201064
Cell-ID™ Intercalator	Fluidigm	Cat#201192A
Cell-ID™ 20-Plex Pd Barcoding Kit	Fluidigm	Cat#201060
Maxpar® Water—500 mL	Fluidigm	Cat#201069
Maxpar® Cell Staining Buffer	Fluidigm	Cat#201068
Maxpar® PBS	Fluidigm	Cat#201058
EQ Four Element Calibration Beads	Fluidigm	Cat#201078
Bond-Breaker TCEP Solution, Neutral pH	Thermo Fisher	Cat#77720
PFA	EMC	50-980-487
Osmium tetroxide	ACROS ORGANICS	319010050
Recombinant SARS-CoV-2 receptor binding domain (RBD)	Krammer Laboratory at the Icahn School of Medicine at Mount Sinai	https://labs.icahn.mssm.edu/krammerlab/reagents/
Recombinant SARS-CoV-2 spike protein (S)	Krammer Laboratory at the Icahn School of Medicine at Mount Sinai	https://labs.icahn.mssm.edu/krammerlab/reagents/
SIGMAFAST™ OPD (o-Phenylenediamine dihydrochloride)	Sigma-Aldrich	Cat#P9187
3-molar hydrochloric acid	Thermo Fisher Scientific	Cat#S25856
Tween-20	Fisher Bioreagents	Cat#BP337-100

Non-fat dry milk Omniblok	AmericanBio	Cat#AB10109-01000
Bovine Serum Albumin Fraction V	Roche	Cat#10735078001
Protein A conjugated magnetic beads	Invitrogen	Cat#10008D
Protein G conjugated magnetic beads	Invitrogen	Cat#10009D
T4 ligase	New England Biolabs	Cat#M0202S
Phusion DNA Polymerase	New England Biolabs	Cat# M0530L
Urea	Sigma-Aldrich	
Ammonium Bicarbonate	Sigma-Aldrich	09830-1KG
Iodoacetamide	Sigma-Aldrich	I1149-25G
Dithiothreitol	Sigma-Aldrich	D9779-10G
LC/MS grade Formic Acid	Thermo Scientific	A117-50
Perchloric Acid	Sigma-Aldrich	311421-50ML
1-Propanol	Sigma-Aldrich	34871-1L
Sera-Mag Speed Beads 65	Sigma-Aldrich	65152105050250
Sera-Mag Speed Beads 45	Sigma-Aldrich	45152105050250
HPLC grade Water	Fisher chemical	W5-4
LC/MS grade Water	Fisher chemical	W6-1
LC/MS grade Acetonitrile	Fisher chemical	A955-1
HPLC grade Methanol	Fisher chemical	A452-4
LC/MS grade Methanol	Fisher chemical	A456-4
LC/MS grade Isopropanol	Fisher chemical	A461-1
Sequence grade Porcine Trypsin	Promega	V5117
K562 Cell Line Tryptic Peptide Mixture Standard 100 µg	Promega	V6951
Trifluoroacetic acid	Sigma-Aldrich	T6508-100ML
Ambion Nuclease-Free Water	Invitrogen	Cat#AM9937
Recombinant human IFNa	R&D	Cat#11101-2
Recombinant human IFNb	Peprotech	Cat#300-02BC
Recombinant human IFNw	Peprotech	Cat#300-02J
Sulfo-NHS	ThermoScientific	Cat#A39269
EDC	ThermoScientific	Cat#77149
Critical commercial assays		
Quick-DNA/RNA Pathogen MagBead	Zymo Research	R2146
RNase-Free DNase Set	Qiagen	79254
NEBNext Ultra II Directional RNA Library Prep Kit for Illumina	New England Biolabs	E7760
AMPure XP Beads	Beckman-Coulter	A63882
Quick-RNA MagBead Kit	Zymo Research	R2133
SMART-Seq v4 Ultra Low Input RNA Kit for Sequencing	Takara Bio	634894
Nextera XT DNA Library Preparation Kit	Illumina	FC-131-1096
DNA Prep, Tagmentation	Illumina	20018705
Chemagic Blood 400 (96) kit	Perkin Elmer	CMG-1091
Global Diversity Array (GDA)	Illumina	20031810
Covaris E210	Covaris, LLC.	10521
T7 Select 10-3b Cloning kit	EMD Millipore	EMD Millipore
AMPure XP Beads	Beckman Coulter	Cat#A63881
Olink Target 96 Inflammation Reagent Kit	Olink Proteomics	Cat#95302, Lot#B02101
Deposited data		
Experimental models: Cell lines		

Expi293F cells	Thermo Fisher	Cat#A14528
Experimental models: Organisms/strains		
Oligonucleotides		
2019-nCOV_N1-F GAC CCC AAA ATC AGC GAA AT	Integrated DNA technologies	Cat#10006713
2019-nCOV_N1-R TCT GGT TAC TGC CAG TTG AAT CTG	Integrated DNA technologies	Cat#10006713
2019-nCOV_N1-P ACC CCG CAT TAC GTT TGG TGG ACC	Integrated DNA technologies	Cat#10006713
2019-nCOV_N2-F TTA CAA ACA TTG GCC GCA AA	Integrated DNA technologies	Cat#10006713
2019-nCOV_N2-R GCG CGA CAT TCC GAA GAA	Integrated DNA technologies	Cat#10006713
2019-nCOV_N2-P ACA ATT TGC CCC CAG CGC TTC AG	Integrated DNA technologies	Cat#10006713
RP-F AGA TTT GGA CCT GCG AGC G	Integrated DNA technologies	Cat#10006713
RP-R GAG CGG CTG TCT CCA CAA GT	Integrated DNA technologies	Cat#10006713
RP-P TTC TGA CCT GAA GGC TCT GCG CG	Integrated DNA technologies	Cat#10006713
SARS-CoV-2 tilling oligonucleotides for whole genome amplification	Gonzalez-Reiche, et al. 2020	https://doi.org/10.1126/science.abc1917
Recombinant DNA		
Vector pCAGGS Containing the SARS-Related Coronavirus 2, Wuhan-Hu-1 Spike Glycoprotein Gene (soluble, stabilized)	BEI Resources	Cat#NR-52394
Vector pCAGGS Containing the SARS-Related Coronavirus 2, Wuhan-Hu-1 Spike Glycoprotein Receptor Binding Domain (RBD)	BEI Resources	Cat#NR-52309
Human Coronavirus Synthetic DNA	Twist Bioscience	https://www.twistbioscience.com
Software and algorithms		
CZID Pipeline	Chan Zuckerberg Initiative	www.czid.org
bcl2fastq v2.20.0.422	Illumina	https://support.illumina.com/sequencing/sequencing_software/bcl2fastq-conversion-software.html
FastQC_v0.11.5	Andrew S	N/A
STARv2.4.3a	Dobin et al, 2013	https://github.com/alexdobin/STAR
Qualimap	Okonechnikov et al, 2015	http://qualimap.conesalab.org
Cutadapt_v3.7	DOI:10.14806/ej.17.1.200	https://cutadapt.readthedocs.io/en/stable/
Preseq_v3.1.1	Timothy D and Andrew Smith et al, 2013	https://github.com/smithlabcode/preseq
Samtools_v1.12	Heng Li et al, 2009	http://samtools.sourceforge.net

MultiQC	Philip Ewels	https://multiqc.info
WGCNA R package (version 1.69-81)	Langfelder, Peter, and Steve Horvath. "WGCNA: an R package for weighted correlation network analysis." BMC bioinformatics 9, no. 1 (2008): 1-13.	https://cran.r-project.org/web/packages/WGCNA/index.html
lme4 R package (version 1.1-27.1)	Bates, Douglas, Deepayan Sarkar, Maintainer Douglas Bates, and L. Matrix. "The lme4 package." R package version 2, no. 1 (2007): 74	https://cran.r-project.org/web/packages/lme4/index.html
ordinal R package (version 2019.12-10)	Christensen, Rune Haubo B. "Cumulative link models for ordinal regression with the R package ordinal." Submitted in J. Stat. Software 35 (2018).	https://cran.r-project.org/web/packages/ordinal/index.html
gamm4 R package (version 0.2-6)	Wood, Simon, Fabian Scheipl, and Maintainer Simon Wood. "Package 'gamm4'." Am Stat 45, no. 339 (2017): 0-2.	https://cran.r-project.org/web/packages/gamm4/index.html
ComplexHeatmap R package (version 2.6.2)	Gu Z, Eils R, Schlesner M (2016). "Complex heatmaps reveal patterns and correlations in multidimensional genomic data." Bioinformatics.	https://www.bioconductor.org/packages/release/bioc/html/ComplexHeatmap.html
circlize R package (version 0.4.16)	Gu, Z. circlize implements and enhances circular visualization in R. Bioinformatics 2014.	https://cran.r-project.org/web/packages/circlize/index.html
pvca R package (version 1.30.0)	Bushel P (2021). pvca: Principal Variance Component Analysis (PVCA). R package version 1.34.0.	https://www.bioconductor.org/packages/release/bioc/html/pvca.html

clusterProfiler R package (version 3.18.0)	Guangchuang Yu, Li-Gen Wang, Yanyan Han and Qing-Yu He. clusterProfiler: an R package for comparing biological themes among gene clusters. OMICS: A Journal of Integrative Biology 2012, 16(5):284-287	https://bioconductor.org/packages/release/bioc/html/clusterProfiler.html
Msigdbr R package (version 7.5.1)	Igor Dolgalev (2022). msigdbr: MSigDB Gene Sets for Multiple Organisms in a Tidy Data Format. R package version 7.5.1.	https://igordot.github.io/msigdbr/
ggbeeswarm R package (version 0.6.0)	Erik Clarke and Scott Sherrill-Mix (2017). ggbeeswarm: Categorical Scatter (Violin Point) Plots. R package version 0.6.0.	https://github.com/eclarke/ggbeeswarm
ggpubr R package (version 0.4.0)	Alboukadel Kassambara (2020). ggpubr: 'ggplot2' Based Publication Ready Plots. R package version 0.4.0.	https://rpkgs.datanovia.com/ggpubr/
ggeffects R package (version 1.1.1)	Lüdecke D (2018). “ggeffects: Tidy Data Frames of Marginal Effects from Regression Models.” _Journal of Open Source Software_,*3*(26), 772. doi: 10.21105/joss.00772 (URL: https://doi.org/10.21105/joss.00772).	https://cran.r-project.org/web/packages/ggeffects/index.html

Tidyverse R package (version 1.3.2)	Wickham H, Averick M, Bryan J, Chang W, McGowan LD, François R, Grolemund G, Hayes A, Henry L, Hester J, Kuhn M, Pedersen TL, Miller, E, Bache SM, Müller K, Ooms J, Robinson D, Seidel DP, Spinu V, Takahashi K, Vaughan D, Wilke C, Woo K, Yutani H (2019). "Welcome to the tidyverse." _Journal of Open Source Software_, *4*(43), 1686. doi: 10.21105/joss.01686 (URL: https://doi.org/10.21105/joss.01686).	https://doi.org/10.21105/joss.01686
mHG R package (version 1.1)	Eden, E. (2007). Discovering Motifs in Ranked Lists of DNA Sequences. Haifa. Retrieved from http://bioinfo.cs.technion.ac.il/people/zohar/thesis/eran.pdf	https://cran.r-project.org/web/packages/mHG/index.html
R6 R package (version 2.5.0)	https://github.com/r-lib/R6/	https://cran.r-project.org/web/packages/R6/index.html
impute R package (version 1.64.0)	Hastie T, Tibshirani R, Narasimhan B, Chu G (2023). impute: impute: Imputation for microarray data.	https://bioconductor.org/packages/release/bioc/html/impute.html
limma R package (version 3.46.0)	Ritchie ME, Phipson B, Wu D, Hu Y, Law CW, Shi W, Smyth GK (2015). "limma powers differential expression analyses for RNA-sequencing and microarray studies." Nucleic Acids Research, 43(7), e47	http://bioconductor.org/packages/release/bioc/html/limma.html
boot R package (version1.3.28.1)	Canty A, Ripley BD (2022). boot: Bootstrap R (S-Plus) Functions. R package version 1.3-28.1.	https://cran.r-project.org/web/packages/boot/index.html

ordinal R package (version 2022.11.16)	Christensen, R. H. B. (2022). ordinal - Regression Models for Ordinal Data. R package version 2022.11-16. https://CRAN.R-project.org/package=ordinal.	https://cran.r-project.org/web/packages/ordinal/index.html
ggalluvial R package (version 0.12.5)	Jason Cory Brunson and Quentin D. Read (2023). ggalluvial: Alluvial Plots in 'ggplot2'. R package version 0.12.5. http://corybrunson.github.io/ggalluvial/	https://cran.r-project.org/web/packages/ggalluvial/index.html
Cytoscape (version 3.8.2)	Shannon P (2003) Cytoscape: a software environment for integrated models of biomolecular interaction networks *Genome Research* 13(11):2498-504	cytoscape.org
BioRender	Biorender	biorender.com
SamTools bam2fq (v1.4, v1.2)	Danecek et al, 2021	RRID:SCR_002105
Trimmomatic-toolkit (v0.36.5)	Bolger, A. M., Lohse, M., & Usadel, B. (2014). Trimmomatic: A flexible trimmer for Illumina Sequence Data. *Bioinformatics*, btu170.	RRID:SCR_011848
STAR aligner (v2.4.2a)	Dobin et al, Bioinformatics 2012	RRID:SCR_004463
HTSeq-count (v0.4.1)	Putri et al, 2021	RRID:SCR_011867
Picard (v1.134)	Broad Institute	RRID:SCR_006525
FASTQC (v0.11.3)	Babraham Institute	RRID:SCR_014583
Data.table R package 1.14.2	Dowle, M, et al Data.table R package version 1.14.2	https://cran.r-project.org/web/packages/data.table/index.html
DT R package 0.21	Xue, Yihui, et al. DT: A Wrapper of the JavaScript Library DataTables R package version 0.21	https://cran.r-project.org/web/packages/DT/index.html

E1071 R package	Meyer, D, et al. e1071: Misc Functions of the Dept of Statistics, Probability Theory Group. R package version 1.7-9.	https://cran.r-project.org/web/packages/e1071/index.html
Metabolon Laboratory Information Management System (LIMS)	Metabolon	Metabolon
MassFragment Application Manager	Waters	Waters MassLynx v.4.1 Waters Corp Milford, USA
MetaboAnalyst 5.0	MetaboAnalyst	https://www.metaboanalyst.ca/
Cytutils R package v0.1.0	Amir et al, 2017	https://github.com/ismms-himc/cytutils
Fluidigm software-acquisition, normalization, concatenation v7.0.8493	Fluidigm	https://www.fluidigm.com/products-services/software
Cytobank	Beckman Coulter	https://premium.cytobank.org
Prism 9	GraphPad	https://www.graphpad.com/
R v4.0.2	The Comprehensive R Archive Network	https://cran.r-project.org/
FLASH v1.2.11	Magoc and Salzberg, 2011	https://ccb.jhu.edu/software/FLASH/
Bowtie2 v2.2.7	Langmead and Salzberg, 2012	http://bowtie-bio.sourceforge.net/bowtie2/index.shtml
Samtools v1.11	Li et al., 2009	http://samtools.sourceforge.net/
NCBI BLAST v2.11.0	Altschul et al., 1990	https://blast.ncbi.nlm.nih.gov/Blast.cgi
CD-HIT	Li and Godzik, 2006 Fu et al., 2012	http://weizhong-lab.ucsd.edu/cd-hit/download.php
COVID_pipe (https://github.com/mjsull/COVID_pipe)	mjsull, Gonzalez-Reiche, et al. 2020	https://doi.org/10.5281/zenodo.3775031
Minimap2 v2.17-r941	Li, 2018	https://doi.org/10.1093/bioinformatics/bty191
Shovill v1.1.0	Kwong, Gladman and Goncalves da Silva	https://github.com/tseemann/shovill
Pilon v1.24	Walker et al. 2014	http://doi.org/10.1371/journal.pone.0112963
Canu v2.2	Koren, et al. 2017	http://doi.org/10.1101/gr.215087.116
Prokka v1.14.6	Seeman, 2014	http://doi.org/10.1093/bioinformatics/btu153
Seqkit v2.1.0	Shen, et al. 2016	http://doi.org/10.1371/journal.pone.0163962

Kraken2 v2.1.2	Wood, et al. 2019	https://doi.org/10.1186/s13059-019-1891-0
Skyline v.21.2.1.377	MacCossLab	http://skyline.ms
LabSolutions v.5.97	Shimadzu Scientific Instruments	https://www.ssi.shimadzu.com/products/informatics/labsolutions.html
Perseus	Tyanova, et al. 2016	https://maxquant.org/perseus//
Fluidigm Real-Time PCR Analysis v4.7.1	Fluidigm	https://www.fluidigm.com/products-services/software
Olink NPX Manager v3.3.2.434	Olink Proteomics	https://www.olink.com/products-services/data-analysis-products/npx-manager/
Nextstrain v. 3.2.0	Hadfield, et al. 2018	https://github.com/nextstrain/ncov
Nextclade v. 1.11.0	Aksamentov, et al. 2021	https://doi.org/10.21105/joss.03773
Pangolin v. 1.11.0	O'Toole, et al. 2021	https://doi.org/10.1093/ve/veab064
Baltic v.0.1.6	Dudas, 2016	https://github.com/evogytis/baltic
IQ-TREE2 v.1.6.12	Minh et al, 2020, Hoang et al 2018	https://doi.org/10.1093/molbev/msaa015, https://doi.org/10.1093/molbev/msx281
Other		
Turbovap Evaporator	Biotage	Zymark TurboVap Cat#Z-TLVE
Waters Acquity UPLC	Waters	Waters Acquity
BEH C18 columns	Waters	Waters Acquity 2.1 x100 mm, 1.7 um columns
Q-Exactive with Orbitrap mass analyzer	Thermo Scientific	Cat#IQLAAEGAAPFALGMBDK
HILIC columns	Waters UPLC	Waters UPLC BEH Amide 2.1 x 150 mm, 1.7 um
Hamilton MicroLab Star Liquid Handling Robotic System	Hamilton Company	https://www.hamiltoncompany.com/automated-liquid-handling/platforms/microlab-star
Geno/Grinder 2000	SPEX Sample Prep	Geno/Grinder 2000
NovaSeq 6000	Illumina	N/A
0.45µm filter plates	Arctic White	AWFP-F20022
1000 ul Pipette Tips	Opentrons	991-00005
300 ul Pipette Tips	Opentrons	991-00008
20 ul Pipette Tips	Opentrons	999-00014

10 ul Pipette Tips	Opentrons	999-00014
20 ul Pipette Tips	Axygen	T-20-R-S
200 ul Pipette Tips	Axygen	T-200-C-L-R-S
Sealing tape 96-well Plates	4titude	4ti-0581
25ml Reservoir	Argos	B3125-100
4-well Reservoir	Axygen	RES-MW4-HP
12-well Reservoir	Axygen	RES16MC-12-N
0.5 ml 96-well Plates	VWR	76210-520
0.8 ml 96-well Plates	VWR	76210-524
MACROSpin C18 plates	The Nest Group Inc.	SNS SS18VL
EvoTip	Evosep	EV2008
PepSep LC 8cm column	Pepsep	PSC-8-150-15-UHP-nC - 8 cm nanoConnect column
Shimadzu LC column	Shimadzu	227-32100-02
Captive Spray Emitter (ZDV) 20 µm	Bruker	1865710
Combitips® advanced, Eppendorf Quality™, 0.5 mL	Eppendorf	0030089421
Combitips® advanced, Eppendorf Quality™, 2.5 mL	Eppendorf	0030089448
Combitips® advanced, Eppendorf Quality™, 5 mL	Eppendorf	0030089448
Combitips® advanced, Eppendorf Quality™, 10 mL	Eppendorf	0030089464
EvoSep One	Evosep	EV-1000
Thermomixer	Eppendorf	N/A
timsTOF Pro	Bruker Daltonik GmBH	N/A
Column Oven Sonation PRSO-V2	Sonication lab solutions	PRSO-V2
Nexera Mikros	Shimadzu Scientific Instruments	N/A
LCMS 8060	Shimadzu Scientific Instruments	N/A
Fluidigm Dynamic Array 96.96 GE IFC	Fluidigm	Cat#BMK-M-96.96
Fluidigm Ctril Line Fluid,150ul	Fluidigm	Cat#89000021
Magnetic COOH Beads Region 34	BioRad	Cat#MC10034-01
Magnetic COOH Beads Region 43	BioRad	Cat#MC10043-01
Magnetic COOH Beads Region 63	BioRad	Cat#MC10063-01
Amine coupling kit	BioRad	Cat#171406001